

AD-A041 216

ARNOLD ENGINEERING DEVELOPMENT CENTER ARNOLD AIR FORCE--ETC F/G 20/5
EPA LASER FLAME ANALYZER SYSTEM.(U)
JUN 77 H T BENTLEY, B W BOMAR

UNCLASSIFIED

AEDC-TR-76-150

NL

1 of 1
ADAO41216



AEDC-TR-76-150

AD A041 216



7
12

**DEVELOPMENT OF A LASER VELOCIMETER
SYSTEM FOR FLAME STUDIES**

ARNOLD ENGINEERING DEVELOPMENT CENTER
AIR FORCE SYSTEMS COMMAND
ARNOLD AIR FORCE STATION, TENNESSEE 37389

June 1977

Final Report for Period 1 July 1973 - 8 February 1976

Approved for public release; distribution unlimited.

gt
DDC
RECEIVED
JUL 5 1977
D

Prepared for

ENVIRONMENTAL PROTECTION AGENCY
RESEARCH TRIANGLE PARK, NORTH CAROLINA 27709

DDC FILE COPY

NOTICES

When U. S. Government drawings specifications, or other data are used for any purpose other than a definitely related Government procurement operation, the Government thereby incurs no responsibility nor any obligation whatsoever, and the fact that the Government may have formulated, furnished, or in any way supplied the said drawings, specifications, or other data, is not to be regarded by implication or otherwise, or in any manner licensing the holder or any other person or corporation, or conveying any rights or permission to manufacture, use, or sell any patented invention that may in any way be related thereto.

Qualified users may obtain copies of this report from the Defense Documentation Center.

References to named commercial products in this report are not to be considered in any sense as an endorsement of the product by the United States Air Force or the Government.

This report has been reviewed by the Information Office (OI) and is releasable to the National Technical Information Service (NTIS). At NTIS, it will be available to the general public, including foreign nations.

APPROVAL STATEMENT

This technical report has been reviewed and is approved for publication.

FOR THE COMMANDER

Eules L. Hively

EULES L. HIVELY
Research and Development
Division
Directorate of Technology

Robert O. Dietz

ROBERT O. DIETZ
Director of Technology

UNCLASSIFIED

REPORT DOCUMENTATION PAGE		READ INSTRUCTIONS BEFORE COMPLETING FORM
1. REPORT NUMBER AEDC-TR-76-150	2. GOVT ACCESSION NO.	3. RECIPIENT'S CATALOG NUMBER
4. TITLE (and Subtitle) EPA LASER FLAME ANALYZER SYSTEM	5. TYPE OF REPORT & PERIOD COVERED Final Report, 1 July 1973 - 8 February 1976	6. PERFORMING ORG. REPORT NUMBER
7. AUTHOR(s) H. T. Bentley III and B. W. Bomar ARO, Inc.	8. CONTRACT OR GRANT NUMBER(s)	
9. PERFORMING ORGANIZATION NAME AND ADDRESS Arnold Engineering Development Center (DY) Air Force Systems Command Arnold Air Force Station, TN 37389	10. PROGRAM ELEMENT, PROJECT, TASK AREA & WORK UNIT NUMBERS Program Element 1A2014	
11. CONTROLLING OFFICE NAME AND ADDRESS Directorate of Technology Arnold Engineering Development Center Arnold Air Force Station, TN 37389	12. REPORT DATE June 1977	13. NUMBER OF PAGES 56
14. MONITORING AGENCY NAME & ADDRESS (if different from Controlling Office)	15. SECURITY CLASS. (of this report) UNCLASSIFIED	15a. DECLASSIFICATION DOWNGRADING SCHEDULE N/A
16. DISTRIBUTION STATEMENT (of this Report) Approved for public release; distribution unlimited.		
17. DISTRIBUTION STATEMENT (of the abstract entered in Block 20, if different from Report)		
18. SUPPLEMENTARY NOTES Available in DDC.		
19. KEY WORDS (Continue on reverse side if necessary and identify by block number) <div style="display: flex; justify-content: space-between;"> <div> air pollution combustion flames velocity measurement </div> <div> lasers laser velocimeter optics particle size </div> <div> speed indicators </div> </div>		
20. ABSTRACT (Continue on reverse side if necessary and identify by block number) An electro-optical laser flame analyzer system specifically designed for EPA applications is described. Preliminary studies to establish design criteria included 1) studies of radiation levels at a number of discrete wavelengths corresponding to common laser wavelengths (that is, HeNe, argon ion, and ruby); 2) determination of fringe quality by means of an imaging system and an acoustically driven probe wire; 3) estimates of particle		

UNCLASSIFIED

042550

UNCLASSIFIED

20. ABSTRACT (Continued)

arrival rates for both oil and gas fired flames; and 4) effect of flame turbulence on LV signals. The EPA laser flame analyzer system consists of a specially adapted two-component laser velocimeter. Provisions were made to include, upon completion of development, both interferometric particle sizing and a third component of velocity. The velocimeter system includes a two-dimensional Bragg cell and utilizes frequency discrimination techniques to separate the two orthogonal and velocity components; it has the capability of selecting two velocity ranges for each component. The processing of the velocimeter signals is accomplished through the use of two Doppler data processors developed at AEDC. Data interfacing and management are achieved by means of a multiplexer circuit which insures simultaneous data acquisition between the several possible sources. This feature is best used to require simultaneous velocity components and particle size. Finally, the requirement for a third component of velocity is discussed. A reference beam system based on color separation techniques is proposed for use under the particular situation presented in the EPA "rainbow" furnace.

AFSC
Arnold AFS Tenn

UNCLASSIFIED

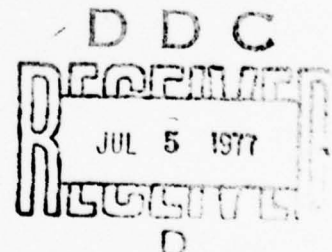
ACCESSION for	
RTIS	White Section <input checked="" type="checkbox"/>
DDC	Diff Section <input type="checkbox"/>
UNANNOUNCED	<input type="checkbox"/>
JUSTIFICATION	
BY	
DISTRIBUTION/AVAILABILITY CODES	
Dist.	AVAIL. AND/OR SPECIAL
A	

AEDC-TR-76-150

PREFACE

The work reported herein was conducted by the Arnold Engineering Development Center (AEDC), Air Force Systems Command (AFSC), at the request of the Environmental Protection Agency, Research Triangle Park, North Carolina, under Program Element 1A2014. The results of the research were obtained by ARO, Inc., AEDC Division (a Sverdrup Corporation Company), operating contractor for the AEDC, AFSC, Arnold Air Force Station, Tennessee, under ARO Project Numbers B32S-11A and BF-406-134A. The authors of this report were H. T. Bentley III and B. W. Bomar, ARO, Inc. The manuscript (ARO Control No. ARO-OMD-TR-76-78) was submitted for publication on July 22, 1976.

The authors are indebted to W. M. Farmer, Spectron Development Laboratories, Tullahoma, Tennessee, and H. R. Bevis, ARO, Inc., for their work on the initial studies of the "rainbow" furnace, which contributed greatly to this report; to T. O. Boiden, Sci-Metrics, Tullahoma, Tennessee, for his design and fabrication of the hardware; to D. W. Roberds, ARO, Inc., for his contributions to the particle-sizing studies; and to A. E. Lennert, ARO, Inc., who furnished guidance throughout the project.



CONTENTS

	<u>Page</u>
1.0 INTRODUCTION	7
2.0 DESIGN CRITERIA	
2.1 Turbulence Effects	10
2.2 Depth of Field	10
2.3 Description of Experimental Apparatus	14
2.4 Experimental Results	16
2.5 Summary of Rainbow Furnace Design Criteria	26
3.0 FLAME ANALYZER SYSTEM DESCRIPTION	
3.1 Self-Aligning, Two-Component Laser Vector Velocimeter	28
3.2 LV Signal Separation and Spectrum Translation System	31
3.3 Optical System	33
3.4 Traverse Assembly	38
3.5 Doppler Processor System	39
3.6 Data Multiplexer	43
4.0 EVALUATION OF THE APPLICABILITY OF INTERFEROMETRIC PARTICLE SIZING	44
5.0 THIRD COMPONENT OF VELOCITY	49
6.0 SUMMARY AND CONCLUSIONS	51
REFERENCES	52

ILLUSTRATIONS

Figure

1. EPA Rainbow Furnace with Photometer	8
2. Location of Furnace Observation Positions	9
3. Optics for Interference Fringe Generation	11
4. Relative Collection Efficiency versus z	13
5. Probe Volume Image Scanner System	15
6. Laser Velocimeter System	15
7. Spectral Radiance as a Function of Wavelength (Fuel Oil at Position I)	17

<u>Figure</u>	<u>Page</u>
8. Spectral Radiance as a Function of Vane Position (Fuel Oil at Position I)	18
9. Spectral Radiance as a Function of Wavelength (Fuel Oil at Position IV)	19
10. Spectral Radiance versus Wavelength as a Function of Furnace Warmup Time	20
11. Spectral Radiance versus Wavelength (Propane Gas Flame)	21
12. Signal Output from Probe Volume Image Scan	22
13. Examples of LDV Signal Distortions	25
14. Two-Dimensional Bragg Cell	29
15. Diffracted Beams from Bragg Cell	31
16. Flame Analyzer Spectra for ± 100 m/sec Velocities	32
17. Signal Separation and Spectrum Translation Systems	33
18. Flame Analyzer Optical System Schematic	34
19. Overview of Optics Showing Forwardscatter Unit	36
20. Photometer System Schematic	37
21. Traverse Assembly Schematic	38
22. Doppler Data Processor Block Diagram	40
23. EPA Flame Analyzer System	44
24. Scattered Intensity for Three Values of D/δ , $z = 0$	45
25. Theoretical Visibility versus Ratio of Particle Diameter to Fringe Spacing	46
26. Theoretical and Experimental Comparison of Visibility versus Ratio of Particle Diameter to Fringe Spacing for a Single Circular Beam Stop	47
27. Proposed Three-Component Velocimeter Schematic	50

TABLES

	<u>Page</u>
1. Particle Velocities in Fuel Oil Flame	23
2. Particle Velocities in Propane Flame (with 60 percent Excess Air)	24
3. Measured Data Rates	24
NOMENCLATURE	54

1.0 INTRODUCTION

The purpose of this report is to outline the basic considerations and principles of the design and operation of the EPA flame analyzer laser velocimeter (LV). The flame analyzer concept was proposed as an aid in the development and evaluation of furnace designs. It also was intended to supplement the use of conventional instrumentation. Areas of application include mixing, burner efficiency, particle dynamics, and verification of mathematical models. The overall program provided not only the resultant hardware (laser flame analyzer) but information concerning the flame environment and the applicability of laser velocimetry and interferometric particle sizing for these areas of research. Specific details will be minimized, and references will be cited for further detailed study. The laser velocimeter designed for the Environmental Protection Agency (EPA) incorporates a number of compromises. For instance, the LV was required to operate under very stringent environmental conditions. At the same time, ease of operation, accuracy, and high data rates were required. The system which was proposed and built represents a good combination of the state-of-the-art technology to give accurate velocity flow-field information within a developmental furnace. The development of a laser interferometer for use as a velocimeter has been well documented as to basic principles and applications (Refs. 1-7) and will not be detailed in this report. Three-dimensional velocity capability was included in the design considerations, but this was not developed. Provisions were made, upon completion of the development of the LV, for simultaneously obtaining particle size information based upon the processing of fringe visibility (Refs. 8-10).

2.0 DESIGN CRITERIA

The EPA "rainbow" furnace is shown in Fig. 1. Basic EPA design requirements were to develop a velocimeter system to: (1) furnish two-dimensional velocity data, (2) incorporate the capability of scanning across the entire furnace core, (3) provide position readout, (4) provide simultaneity of two-component data acquisition, (5) include a provision for the addition of interferometric particle sizing, and (6) design the system with sufficient versatility that a third component of velocity could be added at a later time without major modifications.

The conditions under which the measurements were to be made were unfavorable, at best, as Fig. 2 shows; the velocimeter system

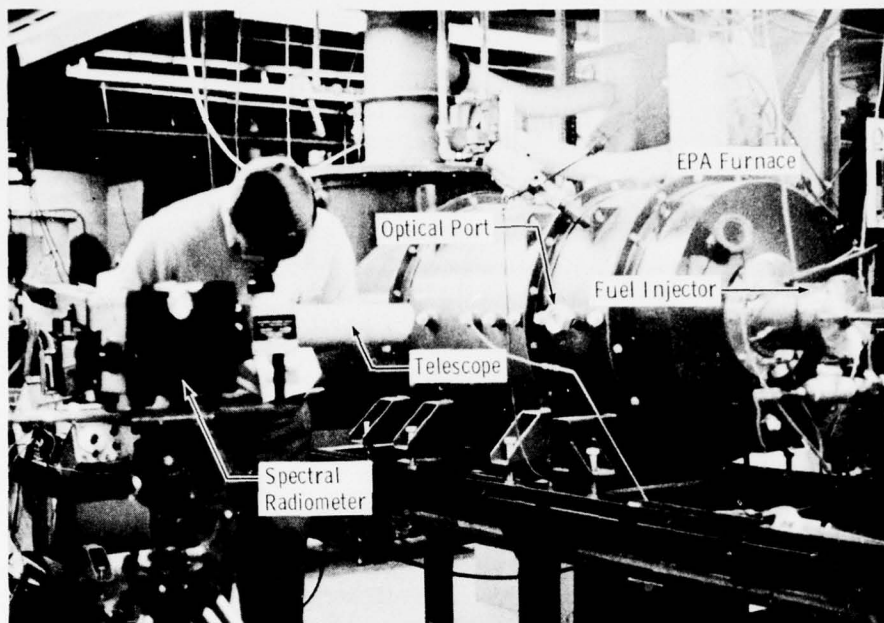


Figure 1. EPA rainbow furnace with photometer.

was to be mated to the EPA furnace observation ports that were 1-1/4 in. in diameter, with a minimum viewing distance from the inner core interface of 7.25 in. Traverse was to be made over a distance of 10.5 in., the inner core diameter. The furnace environment included the presence of fuel oil or gas flames with attendant severe turbulence and density gradients. The background radiation from the flame provided a continuum of unknown opacity. While estimates based on expected equilibrium temperatures could give a measure of the background light level, a high degree of opacity and nonequilibrium effects could greatly modify this finding. Furthermore, the scale and degree of turbulence would affect the formation of high quality probe volume fringes. Therefore, an in situ investigation was made to ascertain the magnitude of these perturbations.

While distortion of the interference fringes in the probe volume of a dual-beam velocimeter could affect signal processing, such distortion would more dramatically affect the particle-sizing instrumentation, the operation of which is based on visibility (Ref. 9). Considering the two

basic LV system operating modes, forward- and backscatter, the latter type is least disturbed by turbulence effects, if the signal intensity level is not considered. In the backscatter mode, radiation must pass backwards over the same optical path it took to reach the probe volume, thereby reducing the effects of beam wander over the phototube aperture. This obviously not the case for forwardscatter systems, as the effects are additive and in no way tend to cancel. For these reasons, a backscatter system appeared to be preferable for the EPA application if the attendant loss in signal intensity level caused by the lower backscatter cross section could be resolved by using a high-powered laser.

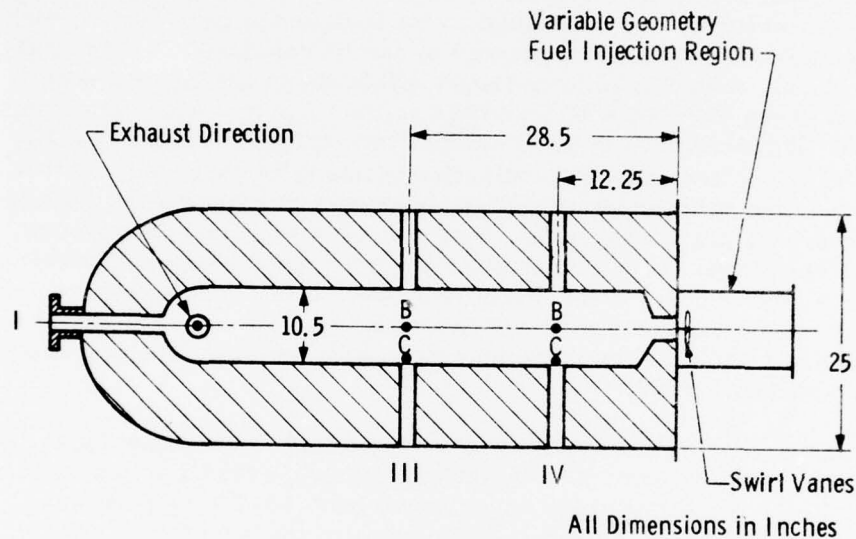


Figure 2. Location of furnace observation positions.

A second reason for selecting the backscatter mode of operation is the simplicity of the optical system. The simultaneous tracking of the transmitting and collection optics system is inherent with the backscatter technique, whereas in the forwardscattering system this is not easily achieved. However, for situations where increased signal strength is required, such as in a gas-fired furnace where the particulates are sparse, a forwardscatter system was designed and built to track with the transmitter, across the probe volume, in one dimension only.

2.1 TURBULENCE EFFECTS

Experiments were performed in the EPA furnace to determine (1) the quality of the probe volume fringes, (2) the quality of the scattered signals, (3) the background radiation levels, and (4) probable data acquisition rates.

Effects of turbulence on beam quality for a dual-beam or dual-scatter velocimeter system have been reported previously (Refs. 11-13). It has been shown that as long as the separation of the beams at the transmitter in the dual-scatter system is, at most, one-half the outer scale of turbulence or equivalent to the turbulence correlation length, relative beam quality is unaffected by the turbulence. That is to say, high quality fringes will be obtained within the probe volume even though gross movement of the probe volume can and will occur because of turbulence-induced index-of-refraction changes. Insofar as the system is unaffected by the collection optics in these cases, neither a forward- nor a backscatter system is greatly affected by the turbulence. However, as previously noted, image wander over an aperture can cause variations in the signal intensity and consequently a distortion of the signal profile. To reduce these effects in a forwardscatter system, a larger aperture must be employed; consequently, more background radiation must be accepted, with the attendant decrease in signal-to-noise ratio.

In the case of local oscillator systems (reference beam type), the scattered wave is perturbed by turbulence as it returns to the collector prior to the mixing with the unperturbed local oscillator reference beam. In this case, the correlation between the wavefronts and the phase variation is destroyed. The net result has been shown to be a limiting aperture effect, beyond which an increase in the collection aperture will not increase the signal-to-noise ratio and in fact may result in a decrease. This is one of the reasons that a reference beam system was not selected for this EPA application.

2.2 DEPTH OF FIELD

To determine the spatial resolution, consideration must be given to those factors affecting the probe volume. The probe volume is normally defined by three criteria: (1) the geometry of the incident radiation, (2) the collection optics and aperture system, and (3) the electronic discrimination.

The first criterion for determining the probe volume is based on the intensity distribution resulting from the interaction of the two crossed Gaussian beams. The one-dimensional velocimeter probe volume, for Gaussian waveforms, has been described (Ref. 2). It was shown that the ellipsoidal probe volume intensity distribution at the $1/e^2$ point (Fig. 3) is given by the following equations:

$$\Delta x(1/e^2) = 2b_o \quad (1)$$

$$\Delta y(1/e^2) = 2b_o / \cos(\alpha/2) \quad (2)$$

$$\Delta z(1/e^2) = 2b_o / \sin(\alpha/2) \quad (3)$$

where α is the angle between the two beams. The characteristic dimension, $2b_o$, is given by

$$2b_o = \frac{4}{\pi} \frac{f_L}{2b} \lambda \quad (4)$$

where f_L is the focal length of the lens, $2b$ is the input beam diameter, and λ is the wavelength of light. (For 125- μ m fringe spacing, a 22-in. focal length lens, and a 3-mm beam diameter, Δz is 60 mm.) Furthermore, the $1/e^2$ equal intensity surface can be shown to be an ellipsoid. The actual volume of this ellipsoid is determined by

$$V = \frac{8}{3\pi^2 \sin \alpha} \left(\frac{f_L \lambda}{b} \right)^3 \approx \frac{8 f_L^4 \lambda^3}{3\pi^2 D b^3} \quad (5)$$

where D is the beam separation at the output lens and $\sin \alpha \approx \alpha = D/f_L$. Particles traversing outside of this region contribute little to the signal intensity.

The sampled probe volume is further determined from the characteristics of the collection lens and aperture system. The effect of a pinhole aperture on the collection efficiency for particles on axis is shown in Fig. 4. Here the collection efficiency is determined for a backscatter system with a 45.7-cm focal length lens. The effective limiting aperture is therefore the pinhole image located at the point $z = 91.4$ cm. Relative efficiency is plotted as a function of distance from the collection lens. It is assumed that the term "geometric optics" adequately describes the system and that the on-axis collection efficiency is also valid in the neighborhood of the aperture image plane.

In practice, this aperture image plane would coincide with the x-y plane of Fig. 3, the probe volume center. The very rapid falloff of collection efficiency as one moves away from the aperture plane is to be noted. A detailed geometric optics evaluation of this characteristic, for both on- and off-axis cases, is found in Ref. 14. (For an aperture image of 1 mm and system f number of 10, the characteristic depth of focus is ± 1 cm.)

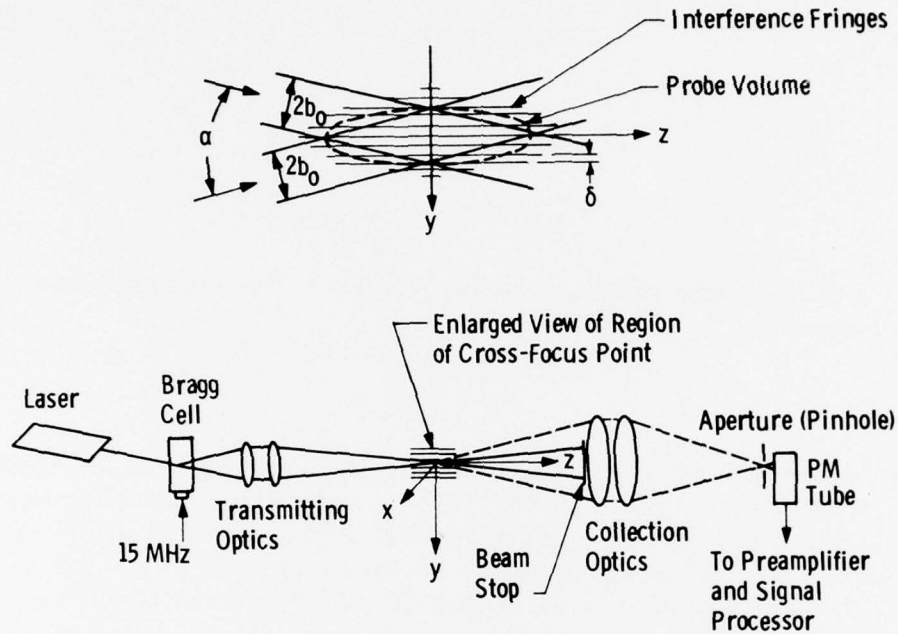


Figure 3. Optics for interference fringe generation.

The analysis of collection efficiency assumes that there is isotropic scattering along the optical axis. This is not strictly the case, as in practice the radiation is strongly lobed in the backward and forward directions in a manner which is dependent upon the particle size, the index of refraction, and the geometry of the particle. Therefore, the particles themselves can contribute to the effective depth of field. In the case of forwardscatter where Fraunhofer diffraction applies, for particles of diameter D , the first minimum occurs at an angle from the axis given by

$$\phi = 1.22 \frac{\lambda}{D} \quad (6)$$

This angle therefore determines an effective collection solid angle for that particular size particle when on-axis collection is being used.

Inherent with the laser flame analyzer design, where the central beam stop (Fig. 3) is located on axis to block the direct unscattered radiation, the overall effect is to increase the relative system response to small particles. The system response, as it relates to particle size processing, is dependent upon the collection lens diameter. The effects of the beam stop diameter will be discussed at greater length in a later section. Electronic discrimination occurs because of low signal to noise ratio near the limits of the depth of field or through the coincidence requirement with other electronics such as a visibility processor. To formulate a mathematical statement of these effects is difficult, at best. The actual effective probe volume is best found experimentally.

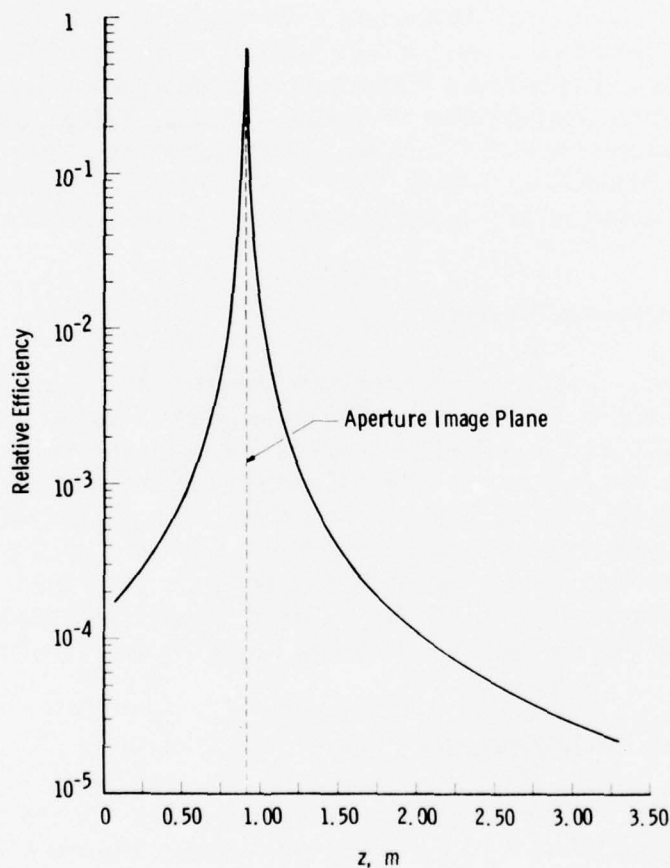


Figure 4. Relative collection efficiency versus z .

2.3 DESCRIPTION OF EXPERIMENTAL APPARATUS

Several preliminary experiments were performed. Radiometric measurements were made to determine the effects of background radiation. The quality of the probe volume fringes was examined to determine the effects of turbulence. Finally, signal quality and data rate were measured. The apparatus is described in the following section.

2.3.1 Spectral Radiometer

The spectral radiometer used in these experiments employed a reflection-grating monochromator which was capable of scanning the visible spectrum from 0.350 to 0.800 μm with a resolution of 0.001 μm . The photodetector utilized an S-20 type photocathode, and the signal values were read with a 3-1/2 digit, digital display. The monochromator was coupled to a photometric telescope equipped with selectable limiting apertures of 6 min, 20 min, 1 deg, and 3 deg. The telescope was capable of a 1-m to infinity focusing range. The radiometer was calibrated for 0.442, 0.448, 0.5145, 0.633, and 0.694 μm against a tungsten ribbon lamp traceable to National Bureau of Standards.

2.3.2 Laser Velocimeter Transmitter

The laser velocimeter transmitter used in the experiments utilized a 15-mw helium-neon (He-Ne) laser operating at 0.633 μm . The laser beam was split into two parallel beams with a glass prism, and the intensities in the beams matched to within 15 percent of each other with a neutral density filter. The probe volume was generated with a 500-mm focal length lens. Fringe period was 17 μm , and the e^{-2} modulation contour probe volume was approximately $2.4 \times 10^{-3} \text{ cm}^3$. The transmitter was mounted on a heavy duty tripod, and the probe volume was positioned in the flame by manual adjustment of the tripod.

2.3.3 Probe Volume Image-Sampling System

To provide information concerning the quality of the probe volume fringes, an image-sampling system was used. Figure 5 is a schematic of the image-sampling system. After passage through the flame, the beams were collected with a lens and brought to focus to form an image of the probe volume. The probe volume image was scanned with a 50- μm tungsten wire. The scanning wire was mounted on the solenoid of an acoustic speaker so that it could be driven across the probe volume

image at a rate determined by an input driving frequency. The light reflected from the wire edge was collected by a lens and focused onto an RCA 931A photomultiplier (PM) tube. The signal current as a function of time was displayed on a storage oscilloscope.

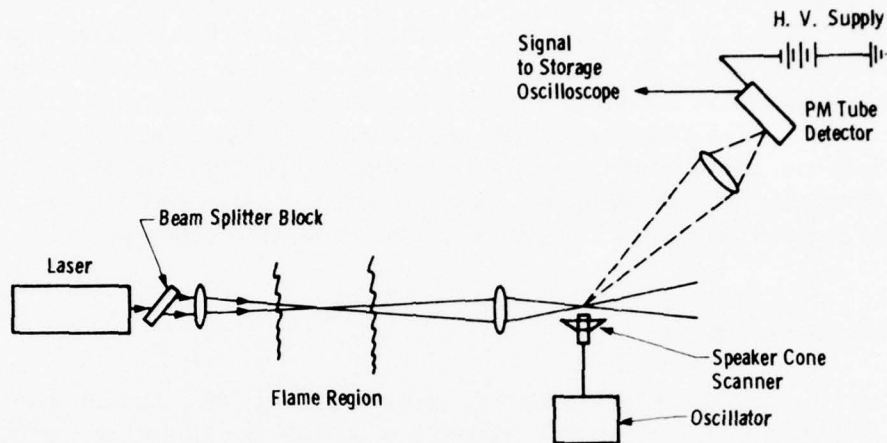


Figure 5. Probe volume image scanner system.

2.3.4 Laser Velocimeter

The velocimeter transmitter described previously was used with the radiometer as a scattered light detector to form a forwardscatter velocimeter system which could be used to observe large scattering particles in the flame. A schematic of the arrangement is shown in Fig. 6. After transmission through the flame the illumination beams pass to a beam stop in front of the photometric telescope. A portion of the scattered light passes around the stops and through the radiometer onto the PM tube detector. The signal from the particle was displayed on a storage oscilloscope.

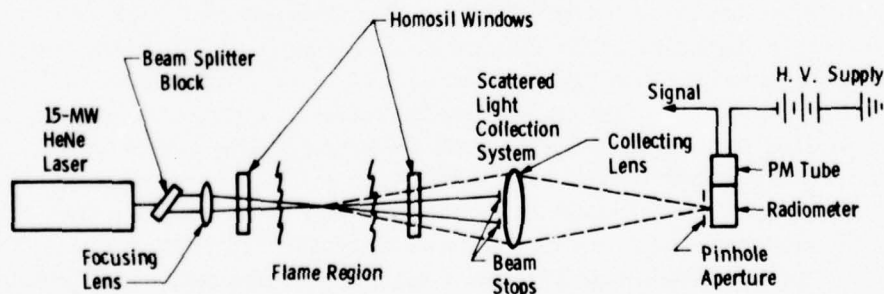


Figure 6. Laser velocimeter system.

2.4 EXPERIMENTAL RESULTS

A schematic of the furnace on which these measurements were made is shown in Fig. 2. Radiometric observations were made on positions I, III, and IV, Band C. Positions III and IV contained ports approximately 1-1/4 in. in diameter. The external ports of these positions comprise Homosil® quartz windows with less than 1/8 wavelength surface distortion and with less than 10 arcseconds of wedge angle between the surface faces. Viewing port I was approximately 3 in. in diameter and of unknown optical quality. Both fuel oil and propane gas flames were observed in these measurements.

2.4.1 Radiometric Results

The results of the radiometric measurements are summarized in Figs. 7 through 11. Figure 7 contains a plot of the spectral radiance of a fuel oil flame as a function of wavelength with the position of the swirl vanes as a parameter, as shown in Fig. 2. The radiometer was focused at position IV-B. Visual observation of the flame showed that it was torroidal in cross section and that the size of the torroid center was a sensitive function of vane position. Thus, there is a considerable variation in the radiance measurements as a function of swirl vane position. It is interesting to note that for a constant wavelength the data, as shown in Fig. 8, reveal a remarkably consistent trend as the vane position is varied. Since spectral radiance is a measure of the energy output of the source it may be concluded either that more particles are being burned at swirl position 6 than at position 5 or that the temperature of the flame has increased considerably. Because of the torroidal shape of the flame, it is suspected that the former possibility is the cause of the variation. The measurements presented in Figs. 7 and 8 were repeated for observation position IV-C, and the results are presented in Fig. 9. There appears to be relatively little radiance dependence on vane position, in contrast to the previous case. The relatively high radiance values and insensitivity to vane position suggest that previous variations were caused by fluctuation in flame shape. Figure 10 illustrates the contribution made to the radiance by furnace walls, as the furnace warms to equilibrium conditions. As expected, the radiant output of the furnace walls can be significant when flame/wall equilibrium is reached. Figure 10 shows that approximately 50 percent of the radiant power produced for the furnace is from the walls, as the effects of window degradation are not significant. Figure 11 summarizes the radiometric observations of a propane gas

flame. Note that the radiance values for the gas flame were significantly lower than for the oil flame; these lower values suggest that there is much less solid material in the flame, as should be expected. Furthermore, visual examination of the gas flame revealed that it was not nearly as opaque as the oil flame.

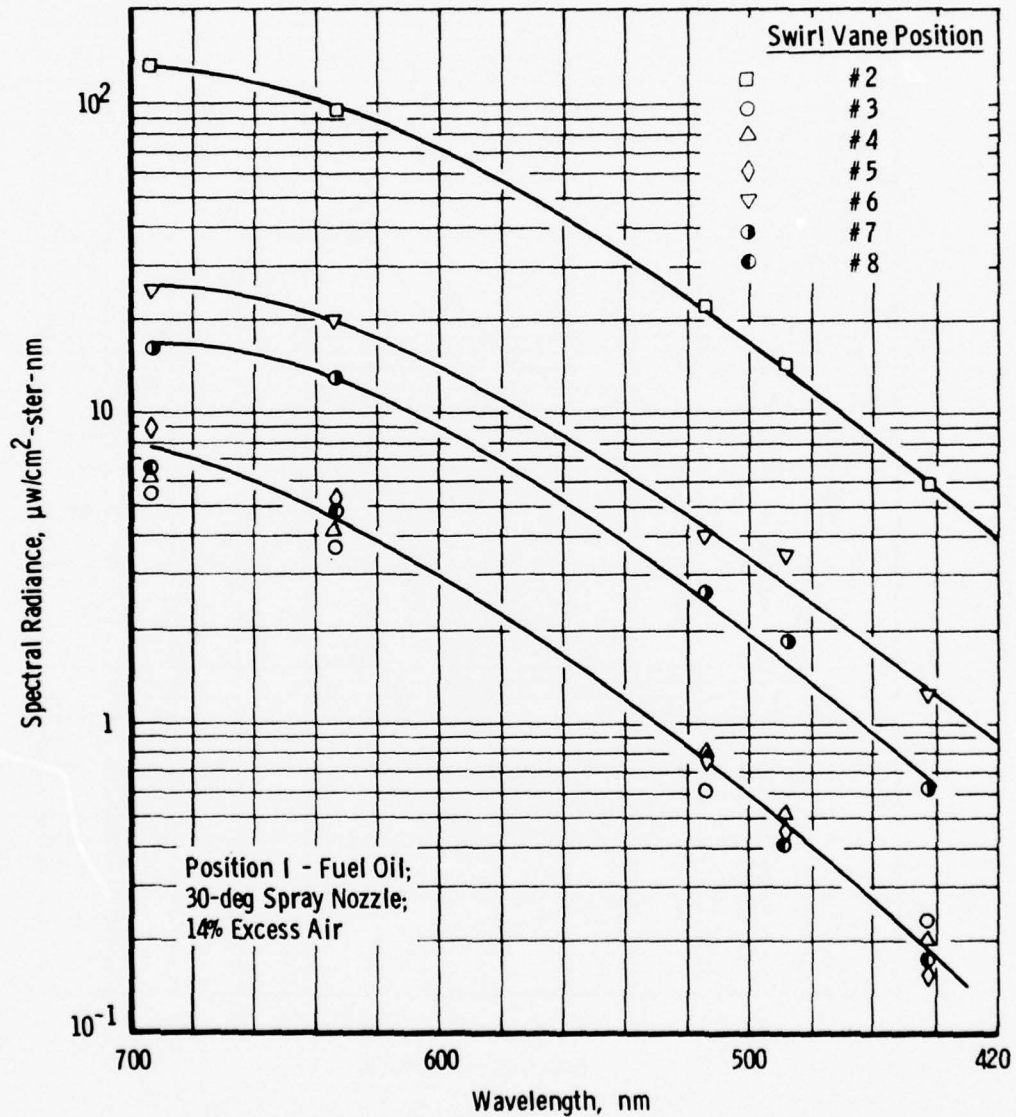


Figure 7. Spectral radiance as a function of wavelength (fuel oil at position I).

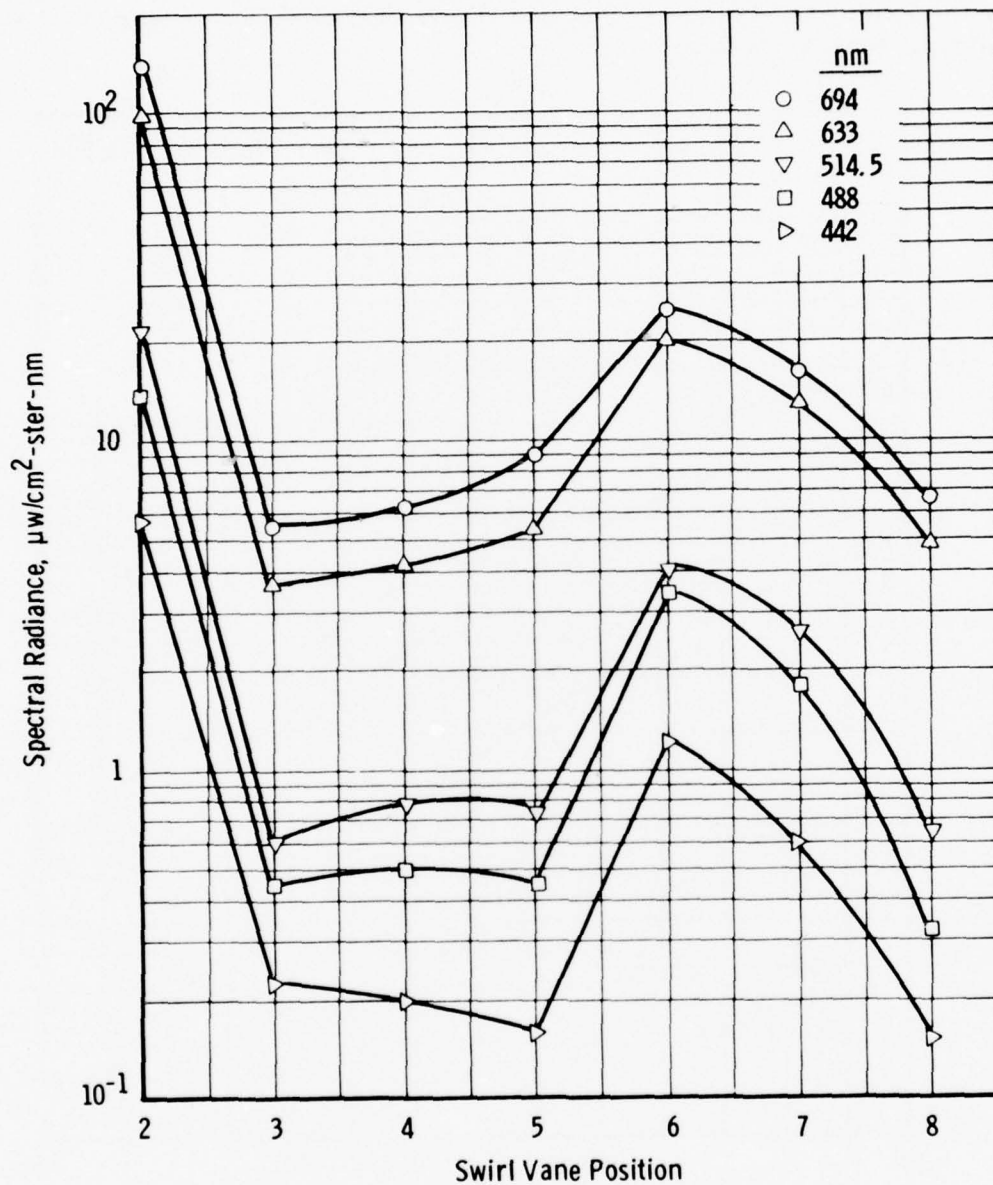


Figure 8. Spectral radiance as a function of vane position (fuel oil at position 1).

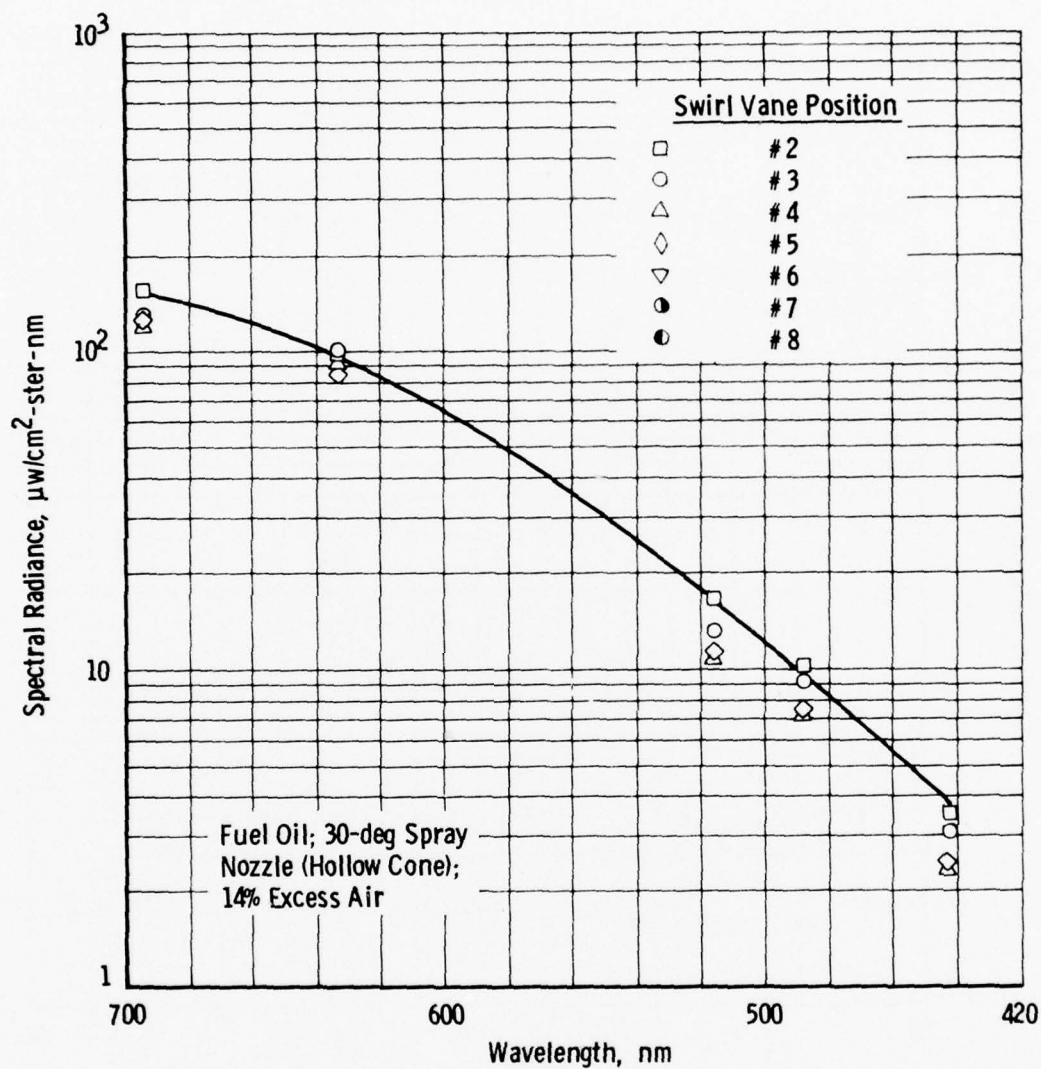


Figure 9. Spectral radiance as a function of wavelength (fuel oil at position IV).

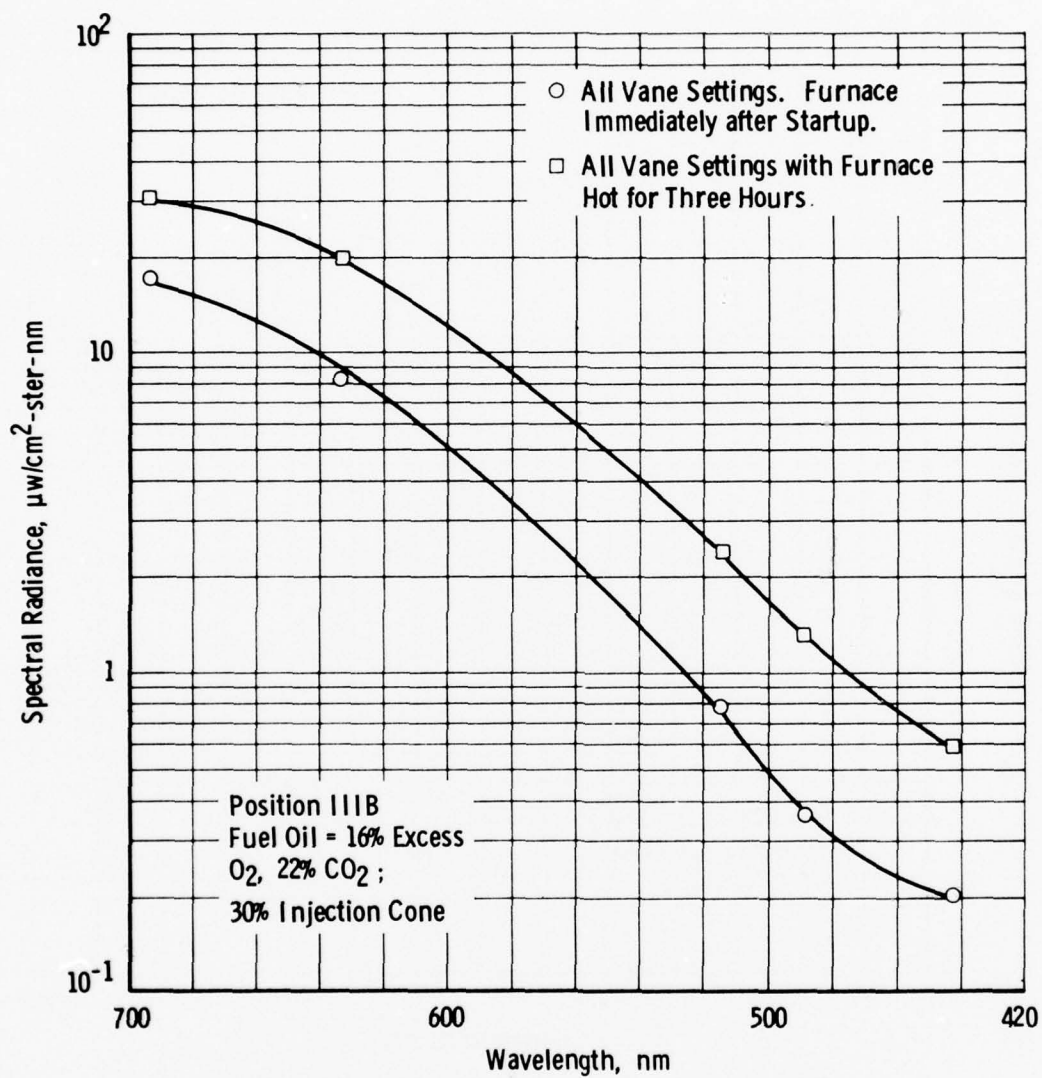


Figure 10. Spectral radiance versus wavelength as a function of furnace warmup time.

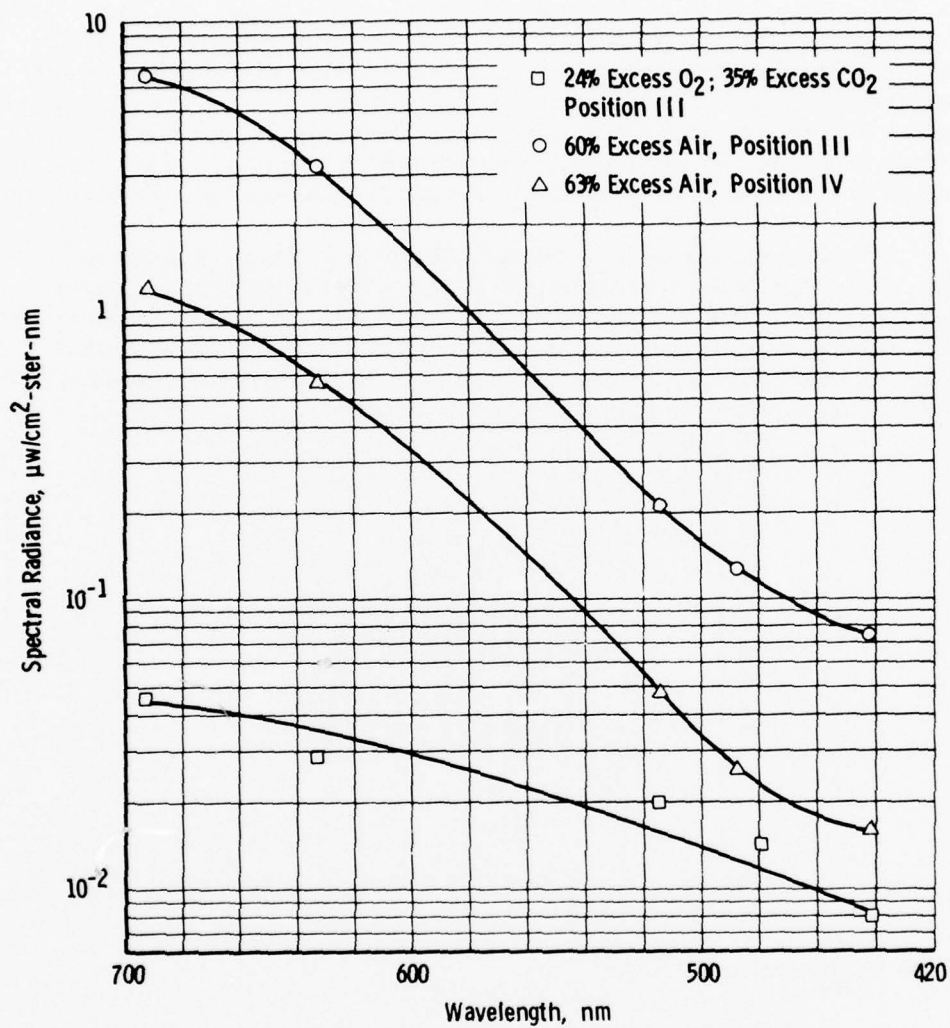


Figure 11. Spectral radiance versus wavelength (propane gas flame).

2.4.2 Probe Volume Image-Sampling System Results

The probe volume sampling system was positioned at observation port IV. The image was sampled at a rate of 15 scans/sec for a large number of flame parameter variations. For this sample rate and a 633-nm wavelength, virtually no changes in the probe volume image could be detected. Figure 12 shows an example of such a scan, taken while the furnace was not in operation. The slight distortion in the image is caused by the optical imaging and scanning system. This signal shape is identical to those obtained when the furnace was in operation.

The data should be interpreted only as indicative, and not as a definitive statement that turbulent distortion of the probe volume is insignificant. The nominal 100- μ sec scan time occupied only about 0.3 percent of the time over which a signal distortion could occur. Particles with longer residence times within the probe volume could be subject to slower-changing turbulence effects.

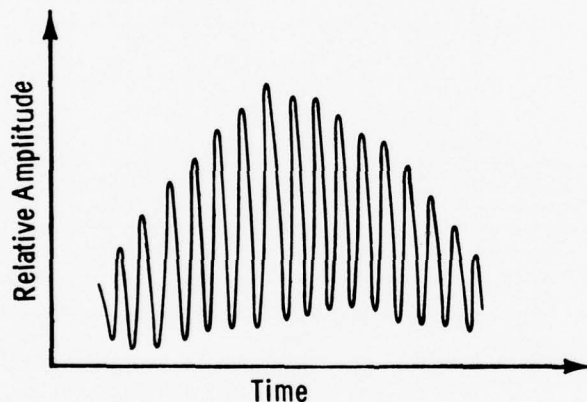


Figure 12. Signal output from probe volume image scan.

2.4.3 Laser Velocimeter Results

The data obtained from the velocimeter observations are summarized in Tables 1 through 3 and in Fig. 13. Both fuel oil and propane gas measurements were made. In order to obtain a sufficient data rate for the observations, it was necessary to utilize approximately 60 percent excess air in the gas flame measurements. Measurements of the fuel oil flame were made at positions IV-B and C, and a large number of scattered light signals were observed. The vast majority of

the signals observed at position IV-B contained little or no velocity information: the fuel droplets were evidently too large for the observational fringe period to produce signals with high visibility. When the observation position was changed to IV-C (i. e., near the edge of the fuel spray), most of the signals again contained no AC information, although some measurable signals did appear. However, at position III-B the sizes of the fuel droplets were much reduced, and a relatively large number of information-carrying signals could be observed. As Tables 1 and 2 show, the velocity of the particles in the oil and gas flames are comparable at positions III-B and C, with the fuel oil probably having a slightly higher velocity. Table 2 shows that the velocity of the particles in the gas flame near the fuel injection region is considerably higher than that observed further down the flame path. In fact, it appears that the particle velocity decreased by a factor of 3 to 4 in a distance of about 15 in.

Table 1. Particle Velocities in Fuel Oil Flame

Measured Particle Velocities, m/sec

<u>Position IIJB</u>	<u>Position IIIC</u>
2.88	1.18
3.76	1.76
4.24	3.82
4.36	4.12
4.72	
4.95	
5.31	
5.9	
6.14	
6.78	
7.08	
7.79	
8.25	
Average: 5.55	2.72

Table 2. Particle Velocities in Propane Gas Flame
(with 60-percent Excess Air)Measured Particle Velocities, m/sec

<u>Position IIIB</u>	<u>Position IIIC</u>	<u>Position IVB</u>	<u>Position IVC</u>
2.35	1.18	11.8	11.3
4.0	1.76	23.6	12.2
4.7	3.23		16.5
	3.82		17.6
	4.12		
Average: 3.683	2.822	17.7	14.4

Table 3. Measured Data Rates
a. Fuel Oil

<u>Data Rate, number/sec</u>	
<u>Position IIIB</u>	<u>Position IIIC</u>
17	19
32	36
	20
	8
Average: 24.5	20.75

b. Propane Gas

<u>Data Rate, number/sec</u>			
<u>Position IIIB</u>	<u>Position IIIC</u>	<u>Position IVB</u>	<u>Position IVC</u>
0.22	0.52	0.74	0.66
	0.32		
Average: 0.22	0.42	0.74	0.66

Data rate measurements were obtained by allowing the oscilloscope to sweep over a relatively long time interval and to record all scattered light pulses. Examples of these values are tabulated in Table 3. Table 3 clearly shows the expected discrepancy in data rate between the gas and oil flames. It should be noted that the data rates recorded in Table 3 are for total input signals into the PM tube. It is estimated that 10 to 20 percent of these signals would provide velocity information and that of those signals perhaps only 20 to 50 percent could be analyzed for particle size. Furthermore, it should be emphasized that the data represent relatively long time averages. Thus, in any specified interval of time the data rate can be considerably higher or lower than the values presented in Table 3. The reason for the large discrepancy in the recorded versus usable data rate lies in the fact that the receiving lens on the radiometer had a relatively large acceptance angle which observed

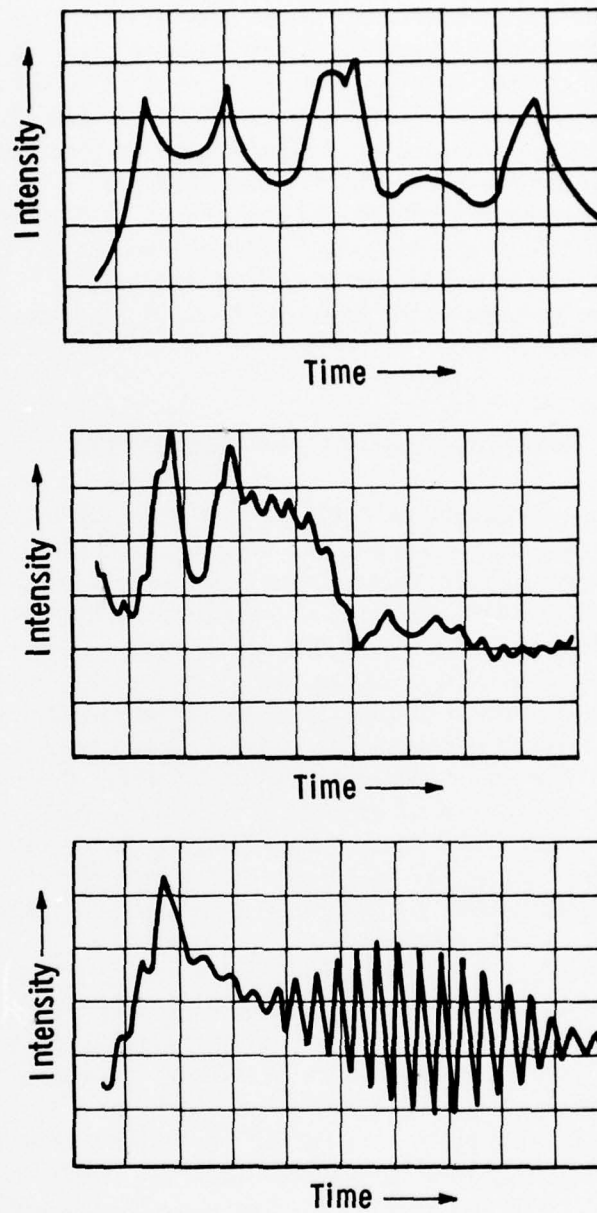


Figure 13. Examples of LDV signal distortions.

not only the probe volume but also light scattered from the individual beams forming the probe volume. Signals were also observed, particularly in the oil flames, that were so distorted as to be virtually unusable. Examples of such signals (which were not unique) are shown in Fig. 13. The mechanism that produces such signals is not presently understood, but the signals could be caused by (1) multiple particles in the probe volume, (2) asymmetric particle shapes, (3) particles changing size and/or shape while in the probe volume, (4) turbulent distortion of the interference fringes, or (5) window contamination, or any combination of the foregoing. Considerable work remains to be done to determine the cause of these phenomena.

2.5 SUMMARY OF RAINBOW FURNACE DESIGN CRITERIA

Radiometric, turbulent distortion, and velocity measurements have been performed on large oil and gas flames. The radiometric measurements show that much less background light exists for light in the blue-green laser lines (0.4880 and $0.5145\ \mu\text{m}$) than in the red lines ($0.6328\ \mu\text{m}$). Since turbulent fluctuations did not appear to have a significant effect on the operation of a velocimeter system for a red line, it appears that a laser line at around $0.500\ \mu\text{m}$ would be a judicious choice for a flame analyzer. Since the argon ion laser offers such a wavelength at the higher power levels required for a backscatter device, the data strongly suggest the use of an argon laser for the EPA application. A $10\text{-}\text{\AA}$, half-bandwidth (HBW) laser line filter will be sufficient for the system when used with a 10- to 15-mw laser velocimeter in a forward-scatter observation mode or a 500-mw (approximate value) laser velocimeter in a backscatter mode.

The velocity data verified that measurements can be obtained in oil and gas flames in a relatively straightforward fashion. For a reasonably high data rate, however, it will be necessary to run the gas flame with a high value of excess air, to supply airborne particles, or with artificially generated scattering particles. Furthermore, in order to obtain velocity measurements near the injector cone for fuel oil flames it will be necessary to employ a probe volume with a large fringe period. The data arrival rate for the oil flames was observed to be reasonably uniform when compared to gas flames as evidenced by the low data rates for propane in Table 3. Observation of the gas flame showed that the scattering particles tended to cluster in pockets, with the result that there were long time intervals over which no data were obtained. When the cluster of particles passes through the probe volume,

the data rate becomes quite high. Such effects can seriously bias the statistics used in determining turbulent velocity characteristics of the air flow in the flame and must be considered in future analyses.

3.0 FLAME ANALYZER SYSTEM DESCRIPTION

The environment to which a laser velocimeter was to be matched and integrated involved regions of recirculation and high degrees of turbulence. In addition, variable amounts of swirl were inherently built into the burner assembly, further complicating the velocity flow field. In cases such as this, where mixing is occurring, reversals in the velocity vector in both space and time are expected. Without a priori knowledge of the flow field, a conventional laser velocimeter, which lacks directionality resolution, would be unable to detect the sign of the velocity vector and would give only the speed. The flow field to be encountered can be assumed to be asymmetric. With a further assumption that the radial velocities are minimal, a two-dimensional, Bragg cell laser velocimeter capable of scanning across the flow field could provide both axial and azimuthal velocity components. The capability for performing higher order correlation, other than the simple velocity mean, requires the simultaneous acquisition of two or more velocity components.

LDV systems can range in complexity from a simple forwardscatter system consisting of a laser, a beamsplitter, a lens, and a collection optics package using an oscilloscope for data analysis for speed measurements, to the sophisticated dual beam system with Bragg cell beam-splitting and frequency separation techniques to provide velocity information. In any system, however, four essential elements are required to obtain velocity field information. They are:

1. A laser source and transmitting and receiving optics.
2. A photodetector, with its associated signal-conditioning and interface electronics.
3. Signal processor and data acquisition electronics.
4. Data processing.

For speed, versatility and accuracy, all phases of the system must perform in an optimum manner.

The first subsystem provides a well defined probe volume and a collection optics system which will collect the scattered light containing the velocity information from the probe volume. For backscatter operation a nominal 2-w argon laser operating at $0.5145 \mu\text{m}$ would provide more than adequate power for most applications operating in the TEM_{00} or Gaussian mode. The net effect of higher order modes is to introduce extraneous frequencies caused by the slight frequency variation from mode to mode. The optics further define the probe volume by transmitting and intersecting the four output beams of a two-dimensional Bragg cell system to a common cross and focal point. For maximum contrast in the fringes, path differences between velocity component beam pairs should be zero.

The propagation of Gaussian beams through optical systems has been discussed in considerable detail (Ref. 15). The effect of a mismatch between the crossover points and the focal point of the individual beams can result not only in a larger probe volume but also in a spreading of the observed frequency spectrum (Ref. 16). This is of particular importance when a turbulent intensity measurement or particle size measurements are to be made. It can be shown that when one is in the far field of the beam waist the fringes form hyperbolic curves in space. This causes a variation in the spatial frequency of the fringes and consequently a variation in the Doppler signal as a function of particle trajectory. The problem is usually found to be more critical when very small fringe spacings and probe volumes are desired (that is, less than or equal to 10λ). A discussion of the parameters influencing this broadening effect in the frequency spectrum is given in Ref. 16.

3.1 SELF-ALIGNING, TWO-COMPONENT LASER VECTOR VELOCIMETER

While most contemporary laser velocimeters utilize the dual beam concept, the Bragg cell-based velocimeter simplifies the optics usually required with the more conventional design. Furthermore, the system is self-aligning and allows two vector components of velocity to be made after initial alignment has been completed. The two-component velocity signals are detected with a single photodetector. Conventional techniques utilizing stationary fringe systems are ambiguous with respect to the flow direction. This directional ambiguity severely limits the use of such instruments in all but the simplest flow field situations (Refs. 1, 17, and 18).

The Bragg cell, dual-beam velocimeter used in the EPA flame analyzer takes advantage of the beamsplitting and frequency-shifting characteristics of a two-dimensional Bragg cell. The beamsplitting characteristics simplify the optical system. The frequency-shifting characteristics separate the two components of velocity into different frequency ranges for detection and analysis.

The two-dimensional Bragg cell (TDBC) consists of two Bragg cells in a common housing arranged such that the centerlines for the cells are coincident and orthogonal (Fig. 14). At the base of each leg is an x-cut quartz transducer disk (Bragg crystal) designed to oscillate in the third overtone. The operating frequencies of the two transducers for the EPA flame analyzer are 15 and 24 MHz.

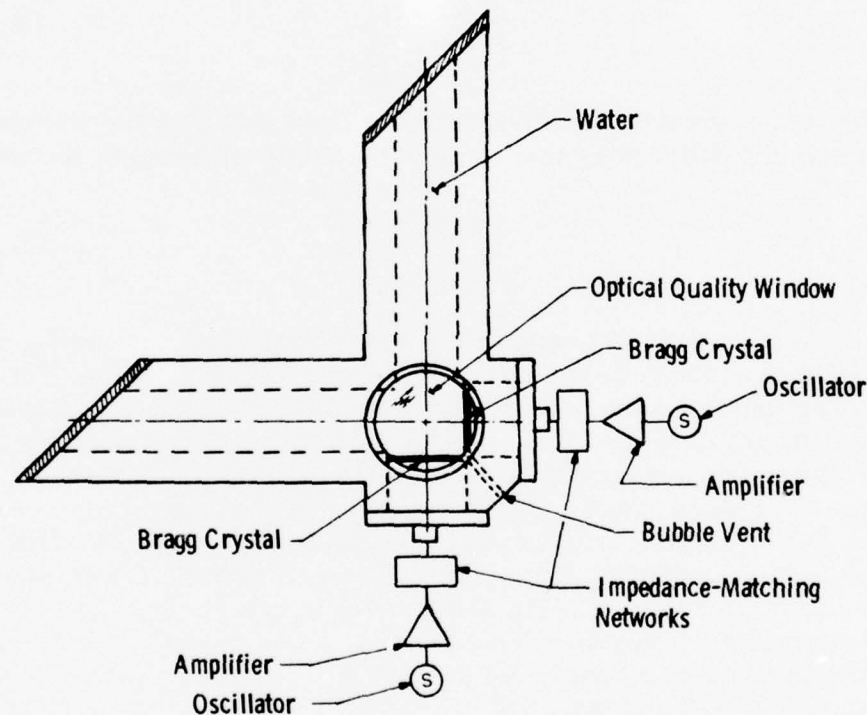


Figure 14. Two-dimensional bragg cell.

Each transducer is driven by a 3-w broadband R-F power amplifier which in turn is driven by a precision crystal-controlled oscillator. Impedance-matching networks are mounted next to the Bragg cell. Their purpose is to eliminate wave reflection at the crystal, reducing

the standing wave ratio and optimizing transducer power requirements (Ref. 17).

The ultrasonic waves propagate through the media, in this case water, giving rise to index-of-refraction variations which may be imagined as two superimposed, linearly independent diffraction gratings moving at a rate equal to the speed of sound in the media (Ref. 19). The diffraction characteristics of the grating are a sensitive function of the orientation of the grating relative to the input illumination. Considering the Bragg mode where half the light is diffracted into a single first order, the angle between the beams, β , satisfies the Bragg equation

$$\sin \beta = \frac{\lambda}{\Lambda} \quad (7)$$

where λ is the vacuum wavelength of the light and Λ is the wavelength of sound in the diffracting medium. The sound wavelength is derived thus:

$$\Lambda = C/f_m \quad (8)$$

where C is the speed of sound in the diffracting medium and f_m is the modulation frequency of the ultrasonic wave (15 or 24 MHz, Fig. 15). The figure indicates the possible frequency combination for several different Bragg orders. The interference fringes generated by any two of the beams are perpendicular to the line joining the centers of the beams. Therefore, taking the four beams in the upper right-hand corner, for example, in addition to the desired 15- and 24-MHz fringes, 39- and 9-MHz crosstalk fringes are also generated. Other diffraction modes are evidenced when the acousto-optic cell is operated in the so-called Raman-Nath region. The deviated beam is shifted in frequency from the undeviated beam by an amount Nf_b , where f_b is the driver frequency and N is the order of diffraction. When a lens is used to bring the beams to a simultaneous crossover in the focus region, or the probe volume, the travelling waves are imaged as moving, mutually orthogonal interference fringes. A scattering particle moving in the same direction as the fringes generates a Doppler frequency less than the moving fringe frequency, f_b . When the particle moves in the opposite direction, the resulting Doppler frequency is higher than f_b .

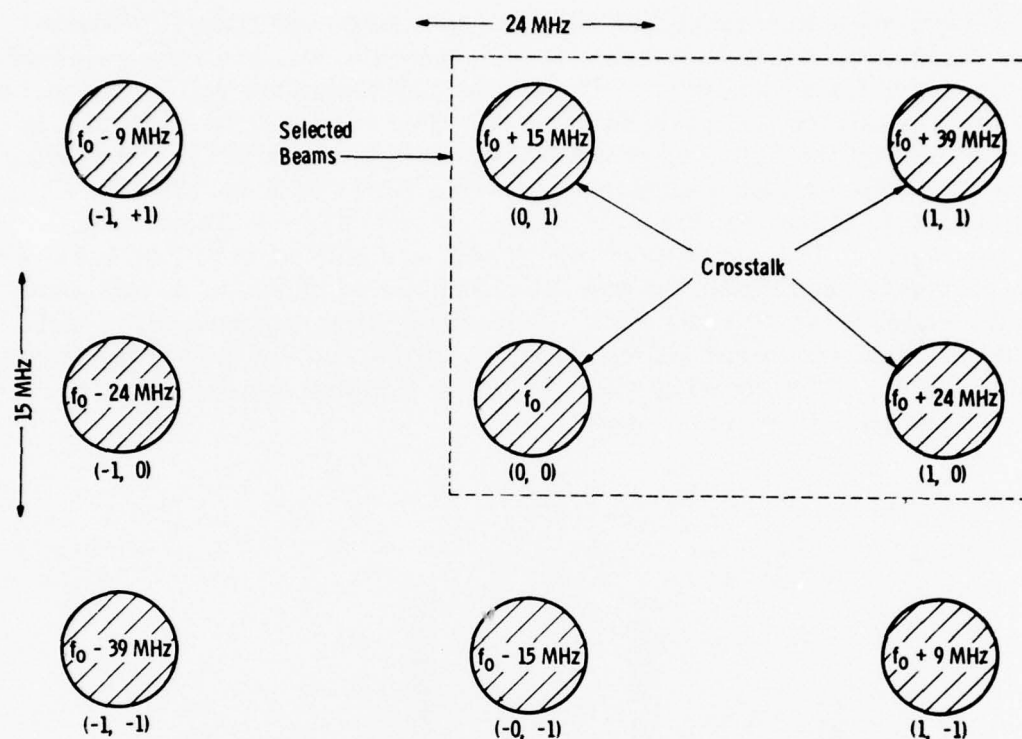


Figure 15. Diffracted beams from bragg cell.

3.2 LV SIGNAL SEPARATION AND SPECTRUM TRANSLATION SYSTEM

The signal from the photomultiplier tube contains the velocity information of both components (Fig. 16) from the information bands I1 and I2. The modulation frequency is centered in the middle of each band at 15 and 25 MHz, respectively. Crosstalk channels 1 and 2, located at 9 and 39 MHz, respectively, correspond to the sum and difference frequencies of the two information bands. Separation of the two information bands prior to processing by the Doppler processor system is accomplished by means of the signal separation and spectrum translation electronics.

Figure 17 shows that the photomultiplier tube output is fed directly to a low noise preamplifier. The gain of the preamplifier is 22 db, with frequency response extending from below 100 KHz to above 100 MHz and a typical noise figure of less than 7 db. The signal is then fed in parallel to each of the two channels for further processing. The input

is a high impedance amplifier followed by a highpass filter. Filters and translation oscillators have been selected to suit the requirements of the laser flame analyzer. The separation technique will be discussed in some detail for the 15-MHz channel. The crosstalk in channel 1 is eliminated by the highpass filtering beginning at 13.8 MHz. Depending upon the velocity range expected, either a 12.7- or a 14.77-MHz oscillator is mixed for the ± 100 m/sec or ± 10 m/sec velocity range, respectively. The corresponding signals are shifted to 2.3 or 0.33 MHz, respectively, and higher frequency crosstalk information is contained in the range from 10 to 54 MHz. A lowpass filter beginning at 5 MHz removes this undesired information, retaining the low frequency Doppler information. The signal is then fed to the Doppler data processor, where the period is determined.

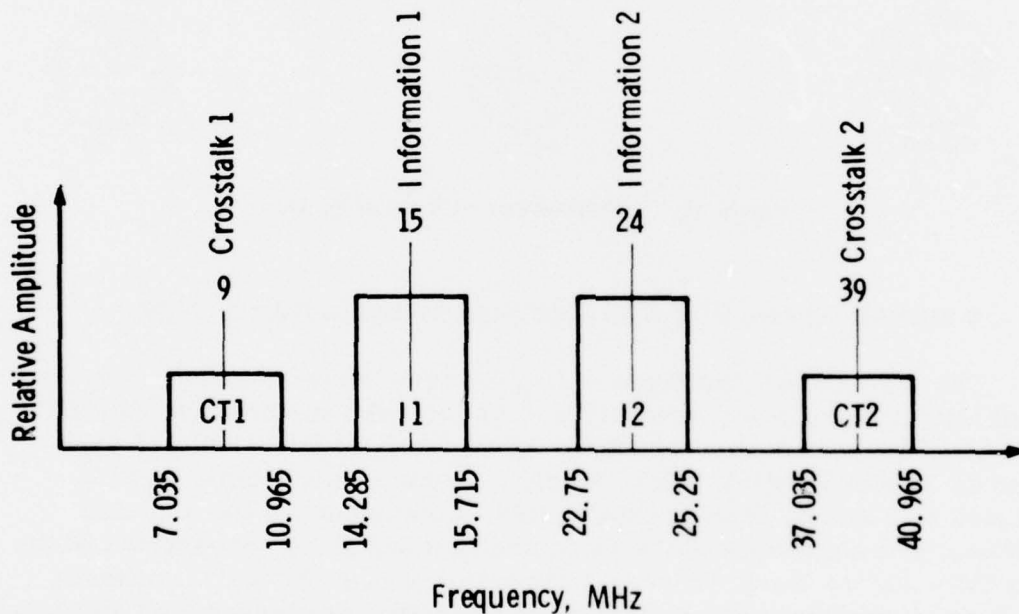


Figure 16. Flame analyzer spectra for ± 100 m/sec velocities.

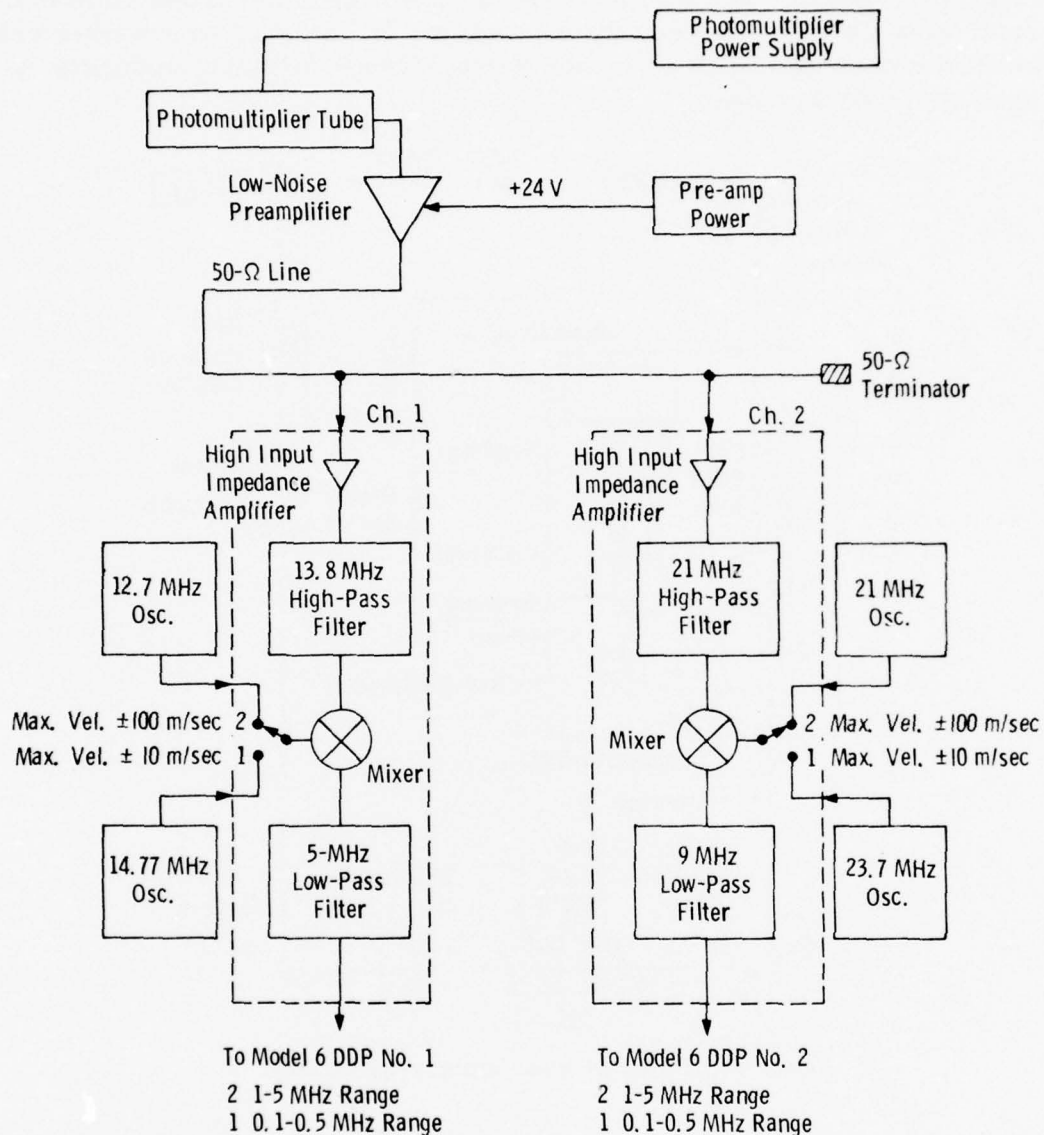


Figure 17. Signal separation and spectrum translation systems.

3.3 OPTICAL SYSTEM

The EPA laser flame analyzer is designed to operate at a wavelength of $0.5145 \mu\text{m}$, which is the predominant wavelength in the argon ion laser

(Fig. 18). Spatial orientation of the fringes within the probe volume to determine the specific velocity components is achieved with a dove prism used in conjunction with a vernier scale. The positioning accuracy is approximately 0.2 deg.

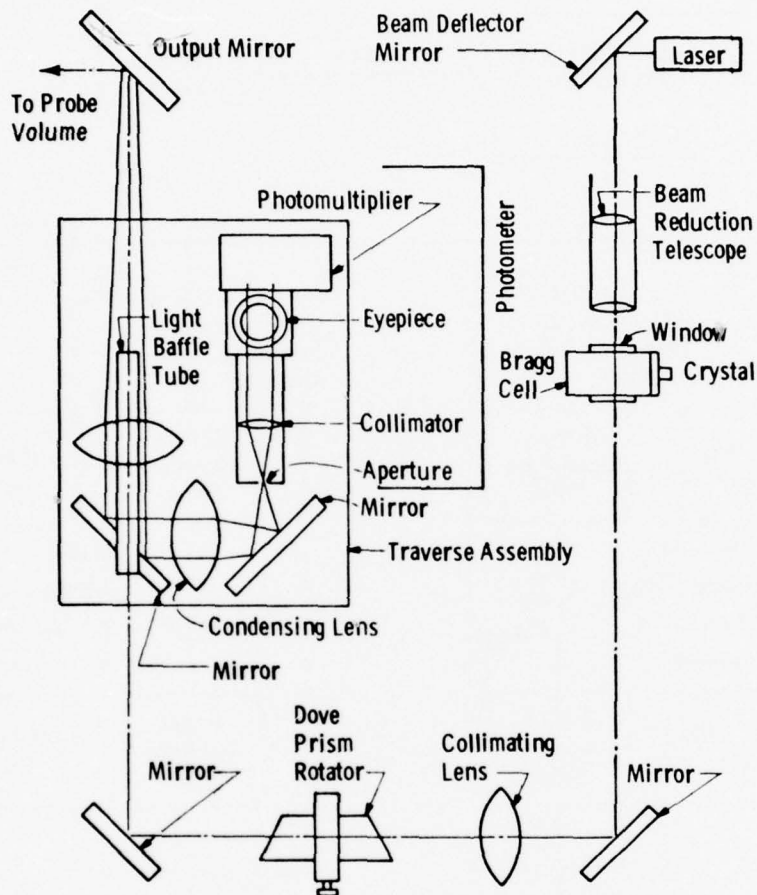


Figure 18. Flame analyzer optical system schematic.

3.3.1 Transmitting Optics

The transmitting lens assembly is capable of positioning the geometric center of the probe volume ± 254 mm (± 10 in.) on either side of the center focus. The position is indicated by means of a digital display. Calibration is accomplished with a zero adjust potentiometer and by varying the power supply voltage to obtain the correct setting. The digital readout is in inches, as measured from any position set by the

zero point adjustment. However, due to restraints imposed by the data multiplexer (to the number of available digits), the recommended scanning range is from 0 to 20 in.

The fringe spacing in the probe volume is given by

$$\delta = \frac{F_P}{F_C} \frac{V}{f_B} = M \frac{V}{f_B} \quad (9)$$

where F_P and F_C are the primary and collimator focal lengths, respectively, V is the velocity of sound in water (1,500 m/sec), and M is the system magnification. The available ranges of fringe spacing are from 114 to 240 μm and from 71 to 150 μm for the 15- and 24-MHz fringes, respectively.

The purpose of the beam reduction telescope is to reduce the laser beam diameter and to properly focus it into the Bragg cell. The size of the beam when focused into the Bragg cell directly determines the beam divergence of an individual beam upon leaving the Bragg cell. The angular separation between the diffracted and undiffracted beams is determined by the modulation frequency [Eqs. (7) and (8)] and therefore affects the probe volume size. The beam reduction optics consist of two lenses spaced approximately the sum of the focal lengths apart. When used in this mode, the output diameter is proportional to the input beam diameter, as is the ratio of their focal lengths as determined by geometrical optics:

$$d_i/d_o = F_i/F_o \quad (10)$$

where d_i and d_o are the input and output beam diameters, respectively, and F_i and F_o are the input and output focal lengths, respectively. As the second lens, the output lens, is also used to focus the beam into the Bragg cell, the distance between this lens and the Bragg cell must be much greater than its focal length.

The collimator lens takes the diverging beams from the Bragg cell and collimates them after they have spread to the desired separation distance. That is, if a larger beam separation is desired, then a longer focal length collimator must be used. The beam separation is determined by the divergence angle (determined from diffraction theory) for the Bragg cell and the focal length of the collimating lens. Increasing the focal length of the collimator will give larger beam

separations, and consequently, upon focusing by the primary lens, one will obtain both a smaller fringe spacing and a smaller probe volume. The collimator, in conjunction with the primary focusing lens, controls the fringe spacing.

The primary focusing lens, or transmitter lens, focuses the beams to form the probe volume. The primary transmitting lens has been cored, the core being replaced, and a light baffle tube used to reduce scattered radiation from its surfaces. This is particularly important at this point due to its close proximity to the phototube collecting optics and the phototube assembly. A 28- and a 36-in. primary focusing lens cell were provided for the EPA system.

3.3.2 Collection Optics

The collection optics in either the backscatter or the forward-scatter mode consists of a collection lens (in the backscatter mode this is also the primary focusing lens) (Figs. 18 and 19). In the

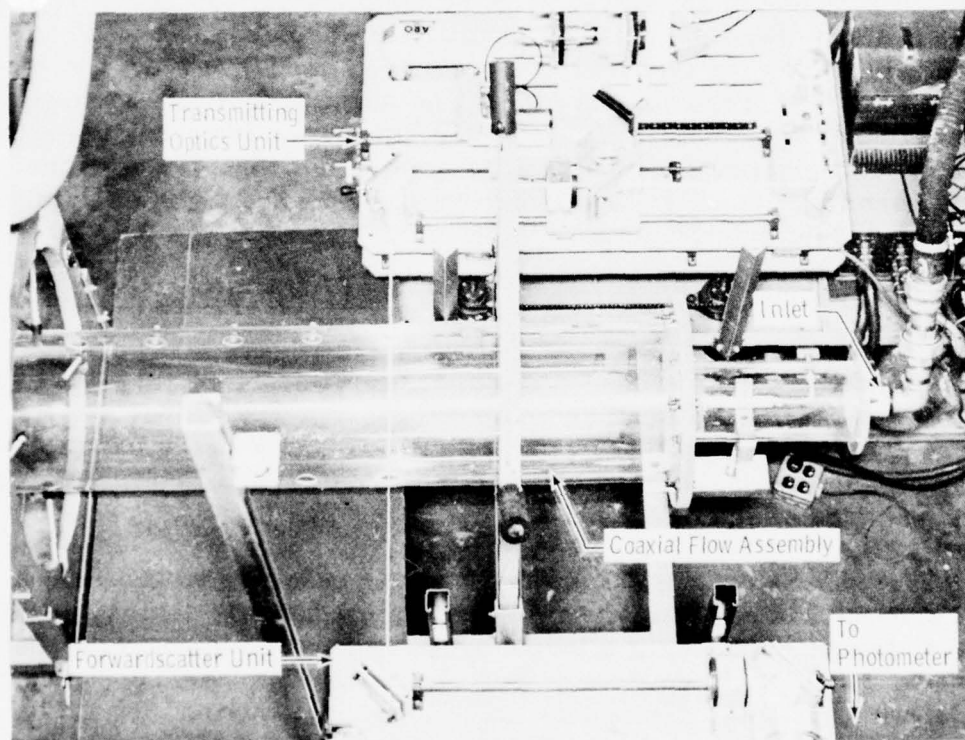


Figure 19. Overview of optics showing forwardscatter unit.

forwardscatter mode the lens is not cored. A condensing lens doublet is located between two mirrors used to fold the optical path for compactness in the backscatter mode of operation. The lens doublet provides a very large aperture and a short focal length condenser. Its purpose is to take the light collimated by the collector lens and to focus it onto the aperture of the phototube assembly. Adjustments can be made in either of the two mirror mounts to obtain imaging of the probe volume into the aperture. These optics, in conjunction with the phototube assembly (photometer), are located on a traverse assembly to give scanning through the region of interest.

The purpose of the photometer is to provide a means of measuring, imaging, viewing, and filtering the scattered radiation from the probe volume in a single unit (Fig. 20). Spatial filtering is provided by

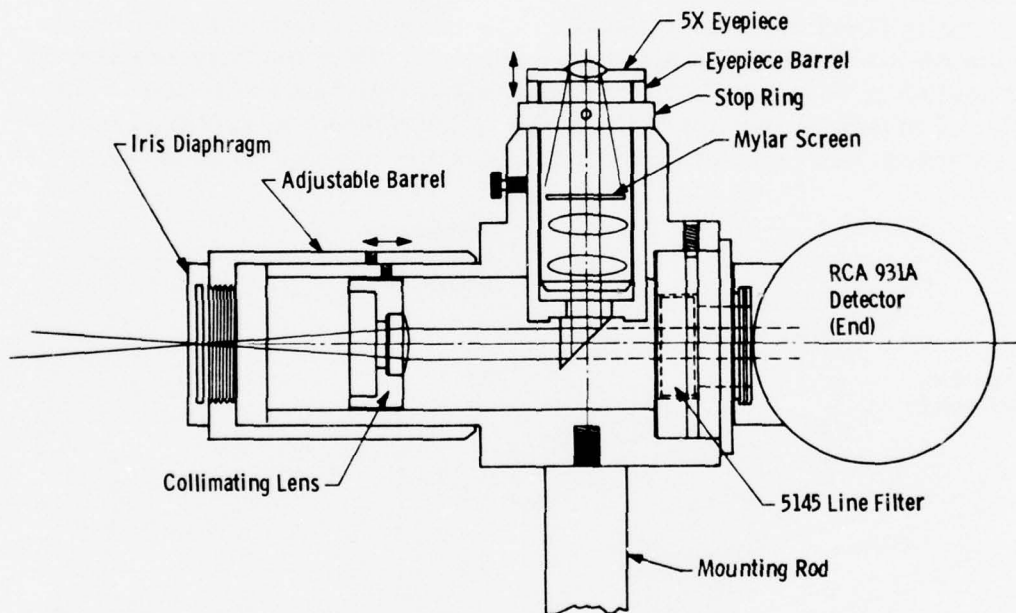


Figure 20. Photometer system schematic.

means of the adjustable entrance iris. The iris can be envisioned as being imaged by the collection optics into the probe volume and acts as the limiting aperture. A collimating lens provides parallel light to the line filter at normal incidence. The $0.5145\text{-}\mu\text{m}$ line filter is $0.0030\text{ }\mu\text{m}$ wide and is critically dependent on angle. A prism can be inserted to deflect the light onto a mylar viewing screen. The eyepiece assembly also can be used to block unwanted radiation from the photodetector.

The photodetector is an RCA model 931A, a rugged phototube with an S-4 response; this peaks at $0.4 \mu\text{m}$. The dynodes are connected to a bridge divider consisting of $100\text{-K}\Omega$ thin film carbon resistors. The first dynodes utilize two 100-v zenier diodes to maintain an optimum voltage. At $1,000 \text{ v}$ the resistor divider will pass 1 ma . A 430-ohm load resistor is provided.

3.4 TRAVERSE ASSEMBLY

The carriage assembly consists of two subassemblies. The base is used primarily as an extender to provide flexibility for use in the various applications (Fig. 21). The base may be separated from the main assembly, as wheels were provided for both. Vertical adjustment was achieved by means of four lead screws driven by sprocket chain and worm gear drive. Since the design requirements were for essentially fixed vertical positions, the assembly was not motorized. To insure stability of the main assembly, the four lead screws are augmented by four angular slide brackets located on each side of the table. Horizontal motion of the table is controlled by another lead screw which can be used to control overall motion by up to $\pm 3 \text{ in}$.

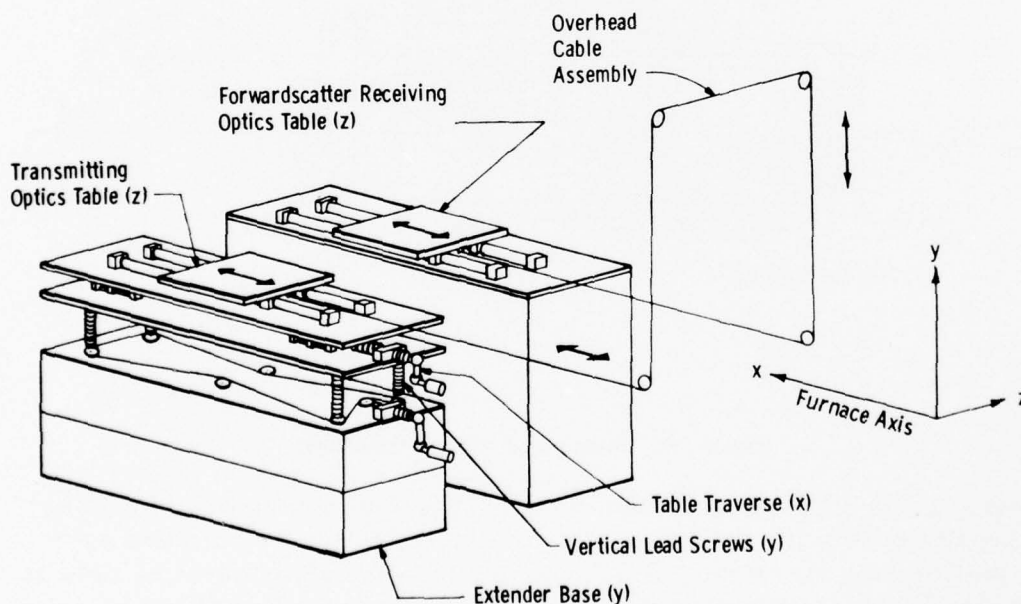


Figure 21. Traverse assembly schematic.

The traverse of the probe volume is obtained by means of a carriage and lens traverse assembly. The traverse assembly consists of a movable carriage, a position readout device, and a small drive motor. The carriage may be moved manually or by means of a small globe-type motor which is directly coupled to the lead screw by means of an O-ring drive belt. The carriage slides onto precisely machined rods straight within one thousandth inch per foot. Contact is maintained by a three-point ball bearing roller assembly. Directional control is determined by two control levers located at the front of the flame analyzer.

The position readout consists of a constant tension spring which is attached to the traverse assembly by means of a cable. The cable makes multiple passes over a drum and drives a 500-ohm potentiometer. Offset voltage is provided through a 100-ohm potentiometer adjustable on the readout device. Power is supplied from a regulated Hewlett-Packard 200 power supply.

3.5 DOPPLER PROCESSOR SYSTEM

The AEDC Model 6 Doppler Data Processor is a sampling device uniquely suited to the analysis of discontinuous signal data. These "frequency first" data arise when the scatter particle density is such that only one particle at a time is traversing the LDV probe volume. This signal type typically occurs when there is no artificial seeding in the flow.

Figure 22 illustrates the Doppler processor in block diagram form. The circuit shown is usable for capture of Doppler burst data over the frequency range from 1 to 500 kHz. A method for extended coverage to frequencies above 500 kHz will be subsequently discussed.

In Fig. 22 the burst data (1) are shown entering the multiband analog filter (2) with simultaneous display on an oscilloscope (3). The filter (2) removes the pedestal (4) and attenuates noise outside the filter pass band. Nine bands, covering 2-1/2 octaves per band, provide an instrument frequency coverage from 1 kHz to 50 MHz. An oscilloscope-triggered gate is used to synchronize the processor sampling interval with the burst signal event displayed on the scope. The scope offers real-time examination of burst signal quality and selective rejection of baseline noise. The processor employs high-speed, emitter-coupled logic, integrated circuit flip-flops (5) and (6) to convert the first eight pulses of Doppler frequency data, after the scope gate (4) opens, into a time interval pulse, the D pulse (39).

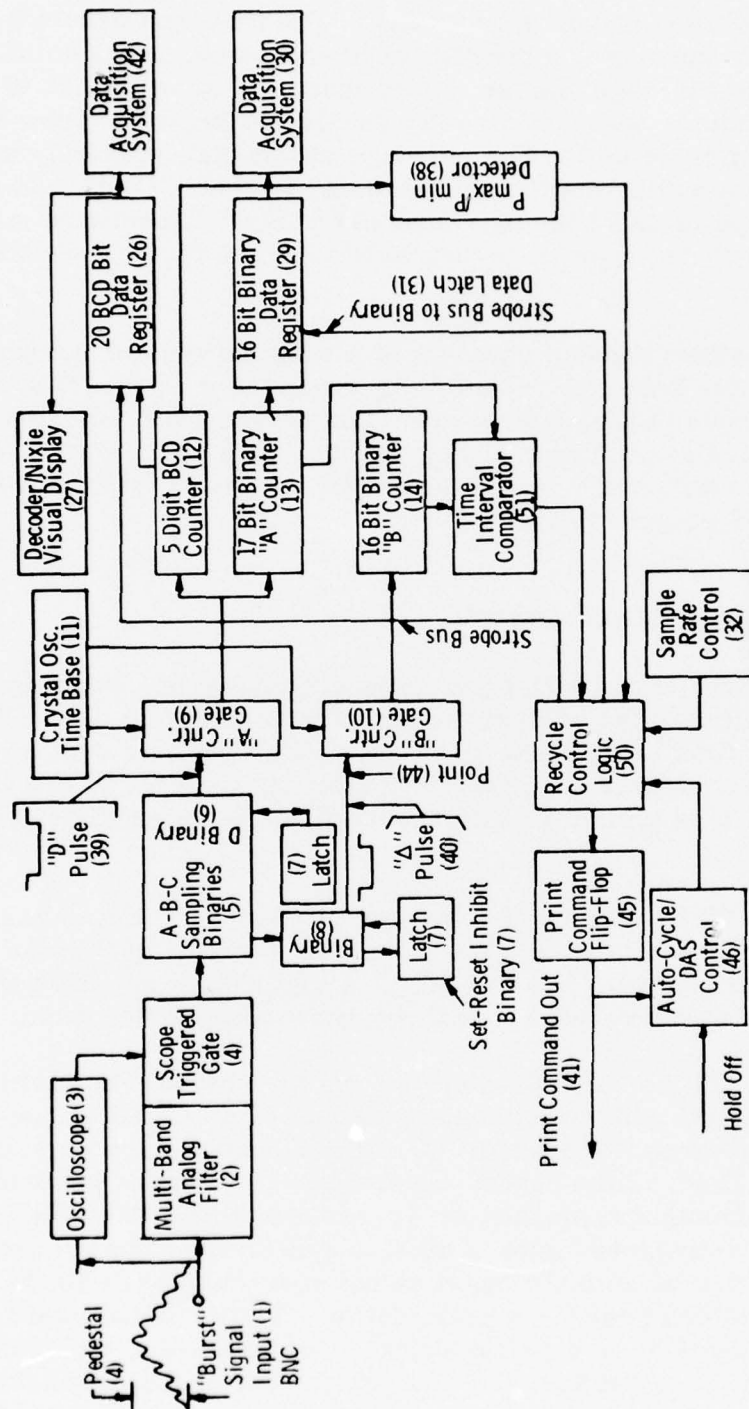


Figure 22. Doppler data processor block diagram.

Simultaneously, a second time interval pulse, called the Δ pulse (40), is generated by the Δ binary (8). The time duration of the Δ pulse is equal to the time period of the first four pulses in the burst signal. The inhibit binary (7) prevents further pulse activity on the part of the D and Δ binaries after the eight- and four-pulse sample interval.

The Doppler processor applies to the two time interval pulses the criterion that if an ideally periodic burst signal were being sampled the time interval of the D pulse would be twice that of the Δ pulse. The processor can make this time interval comparison to better than 0.05 percent of the D pulse interval on those ranges offering adequate time resolution.

The field-operated LDV can produce a variety of signals in addition to the desired Doppler frequency burst signal with acceptable signal-to-noise ratio. Noise bursts, short Doppler signal bursts caused by particle passage through too few fringe lines for accurate transient time resolution, and large amplitude pedestal signals with small Doppler frequency signal amplitudes are typical "problem" signals to be avoided. As an aid in the rejection of such undesirable signal information and in placing limits on the deviations permitted in the signal period averaging, the processor is equipped with a time interval comparator. The comparator functions to compare twice the time interval of the Δ pulse (40) to the D pulse (39). A preselected percentage of the D pulse is used as a limit detector against which the double- Δ pulse is compared. Only double- Δ pulses that lie within the accepted percentage of the D pulse time interval are accepted as period data. The D pulse interval percentage value forms a time interval "data window." Signal quality versus signal quantity trade-offs have arrived at data window values of 1-1/2 or 3 percent of the D interval.

Doppler signal input is accomplished by means of two BNC jacks, one covering the burst signal range from 1 KHz to 20 MHz with a threshold sensitivity (minimum Doppler pulse amplitude acceptable) of 2 mv RMS and input impedance of 100 K Ω , input signal amplitude limited to 1 v peak-to-peak. The second jack covers the range from 10 to 50 MHz with a threshold sensitivity of 3 mv RMS and an input impedance of 50 Ω . Two 50- Ω BNC jacks permit monitoring the sampled signal at the filter output.

The BNC connector requires a positive edge (minimum 0- to 5-v signal, maximum 30-v signal) in synchronism with the initiation of an oscilloscope sweep. The scope is set to trigger on the leading edge of signal bursts with minimum triggering on the signal source baseline noise. Scope bandwidth and gate trigger-rise time must be correlated to the burst signal frequency to be sampled. For well characterized, known areas of LDV application where routine data taking is being performed, the scope may be replaced by a voltage comparator having a suitable rise time. The scope provides a valuable real-time display of the signal quality (signal-to-noise ratio approximation), relative signal amplitude to the processor minimum threshold signal requirements, and the assurance that the processor is sampling frequency bursts a large portion of the time, not random noise sources. An approximation of the burst signal frequency is available from the scope display, which is useful in the selection of the appropriate processor frequency band.

A solid-state LED produces a nominal 60-msec flash each time the processor completes a sample interval. The lamp functions whether data transfer is effected during the sample or not. The lamp is a visual check that the two necessary conditions for processor sampling have been met, namely: (1) that the burst signal amplitude is above the minimum threshold value and (2) that the proper +A gate signal has been furnished.

A five-digit Nixie array (27) displays the period of the Doppler frequency directly in units of microseconds for the five lower frequency ranges, covering from 1 to 500 KHz, and in nanoseconds for the upper 0.4- to 50-MHz ranges, the pulse-stretched range. Data are available in either BCD (26) or binary form (29) to an external data acquisition system (42 and 30, respectively).

Print command generation (41) by the print command flip-flop (45) is under the control of the recycle logic (50). The logic also generates the strobe to output the data from the data registers (26 and 29). The P_{\max}/P_{\min} circuit (38) inhibits the recycle logic if the data exceed the preselected frequency range. The sample recycle rate is controlled by (32). The processor can operate independently of a data acquisition system by routing the print command back as a hold-off pulse (46).

3.6 DATA MULTIPLEXER

The purpose of the data multiplexer is to coordinate operation of the various flame analyzer data sources and arrange the data in a format acceptable to a data acquisition system. Coordination of the data sources (two AEDC Model 6 Doppler Data Processors, a visibility processor, and a traverse position readout) is accomplished by gating the multiplexer with the scope +A gate and allowing the multiplexer to gate all data sources simultaneously via its gate output.

The data sources required for a given set of measurements are selected by programming appropriate data select switches on the front panel of the multiplexer to an up position. At least one data source is required to initiate the data validation and data transfer cycle.

Following the gating of all data sources, the multiplexer waits an interval of time, nominally 900 msec, for all units to complete a measurement. A logic network within the multiplexer then determines if validated record commands have been received from the required data sources. Validated data therefore were measured and processed within the multiplexer settle time.

If all required sources have provided record commands, the multiplexer proceeds to output data from those sources along with any other data which may exist from nonrequired sources. Nonrequired data sources which failed to obtain readings at a given scope gating will have zeroes output for their readings (zero would never be a valid reading from any required source).

Traverse position is the only data source which will always have a measurement ready to be output following each scope gating. The three other data sources make a determination of whether or not to provide data from a given burst waveform based on such parameters as signal-to-noise ratio and particle acceleration.

If any of the required data sources selected on the multiplexer fails to provide a reading after 900 msec from a given gating, all data sources are reset for another sample attempt. This resetting is accomplished by applying and terminating a hold-off pulse to each data source. The EPA flame analyzer system is shown in Fig. 23 exclusive of the traversing forwardscatter unit previously shown (Fig. 19).

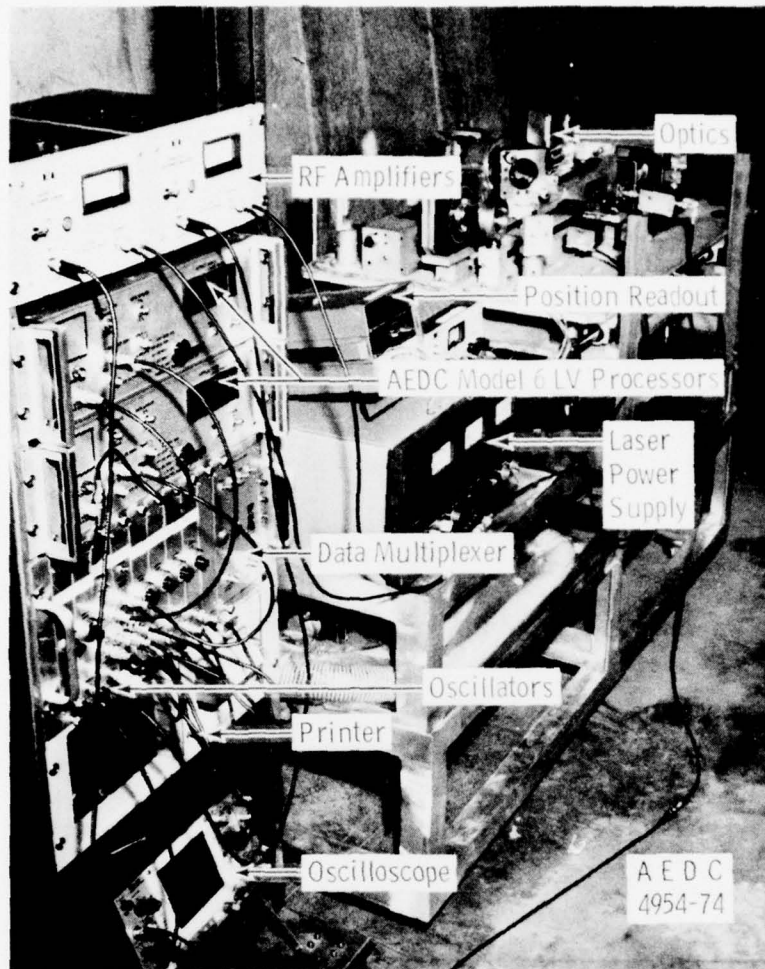


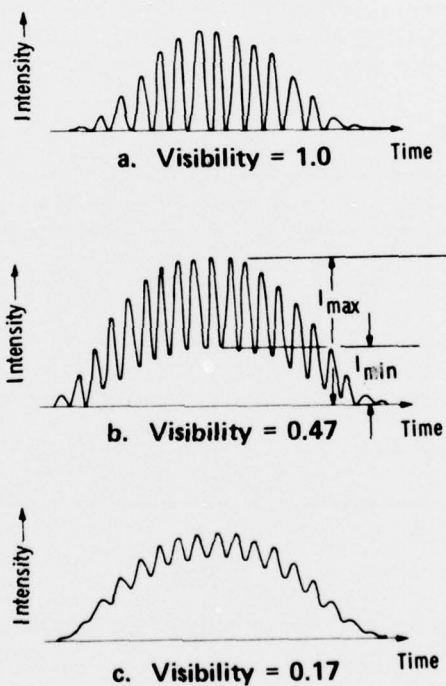
Figure 23. EPA flame analyzer system.

4.0 EVALUATION OF THE APPLICABILITY OF INTERFEROMETRIC PARTICLE SIZING

Including an interferometric particle-sizing capability with the velocimeter system will offer the capability of measuring not only the velocity but also the size of the particle whose velocity is being measured. The interferometric particle-sizing technique has a distinct advantage in that it is independent of the absolute magnitudes of scattered light; furthermore, it uses the same optical system as that of the velocimeter (Ref. 20). This affords the opportunity of making simultaneous velocity and particle size measurements. A prototype electronic

signal processor has been designed and built and is currently being calibrated in the laboratory. With the successful development of the technique, it will be possible to provide rapid, online data acquisition of particle sizes.

The operation of the technique can be briefly summarized by referring to Fig. 3. When a particle crosses a set of interference fringes formed at the crossover point or focal volume of the two laser beams, light is scattered by the particle and collected by the receiving optics, where it is focused onto a photomultiplier tube. The characteristic waveforms evidenced by the particle traversing the focal region is sketched in Fig. 24. In this particular figure, Doppler bursts of particles moving in the y-direction and through the $z = 0$ plane are depicted. It can be seen from the figure that the waveforms consist of a Gaussian modulated cosine component, called the "ac", in addition to a lower frequency Gaussian waveform, or "dc", called the "pedestal."



$$\text{Visibility} = \frac{(I_{\max} - I_{\min})/2}{(I_{\max} + I_{\min})/2}$$

Figure 24. Scattered intensity for three values of D/δ , $z = 0$.

The so-called visibility of the point on the waveform is defined as the ratio of the magnitude of the ac component (one half the peak-to-peak value) to the value of the dc pedestal at that point. The value of the visibility is a function of the ratio of the particle size to the fringe spacing. The characteristic signal is also a function of the particle location within the probe volume and the geometry of the collecting optics. In Figure 25 the theoretical relationship between the visibility and the ratio of particle-to-fringe spacing (d/δ) is plotted. In this particular figure the forwardscattered light is collected for a spherical particle in either the $y = 0$ or $z = 0$ plane. Figure 26 shows experimental and theoretical comparison for a single, circular, 1.55-cm beam stop radius with a 5.5-cm collection aperture radius. Fraunhofer diffraction theory was used to predict the on-axis visibility values.

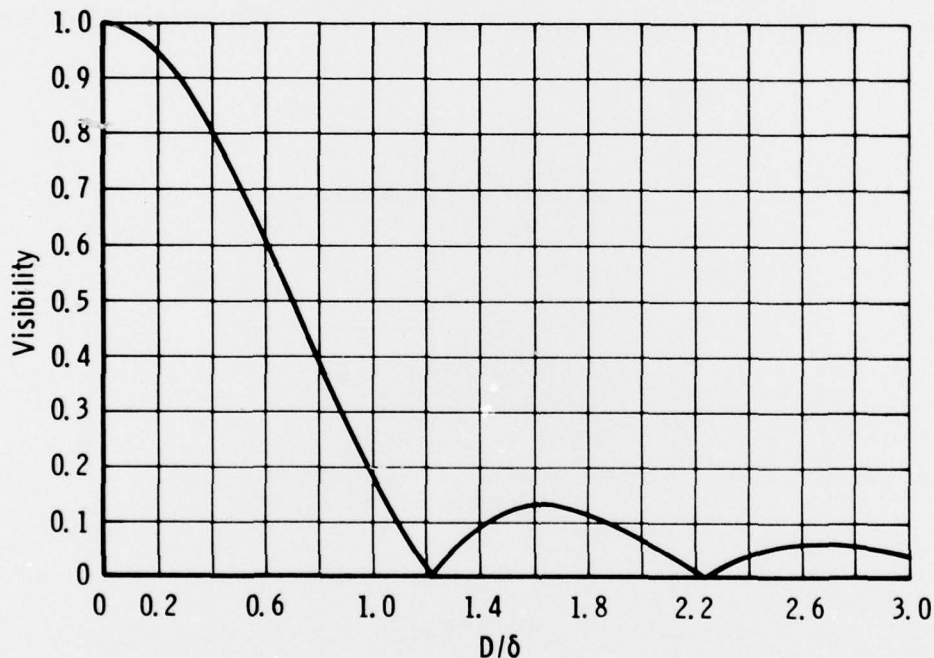


Figure 25. Theoretical visibility versus ratio of particle diameter to fringe spacing.

The following considerations must be taken into account in order to apply this technique of particle sizing to a given environment.

1. In the one-dimensional case, spherical particles are assumed in the event the actual particle shapes are unknown. In this

manner, it is possible to obtain a first order approximation to the size of the particle being measured. By including a second visibility measurement using an orthogonal fringe set (such as is used for the two-component velocimeter), a check can be made on the accuracy of the particle size, including a confirmation of whether or not the particles are indeed spherical. In the event the visibility differs for each of the two so-called visibility components, nonspherical shape must be assumed.

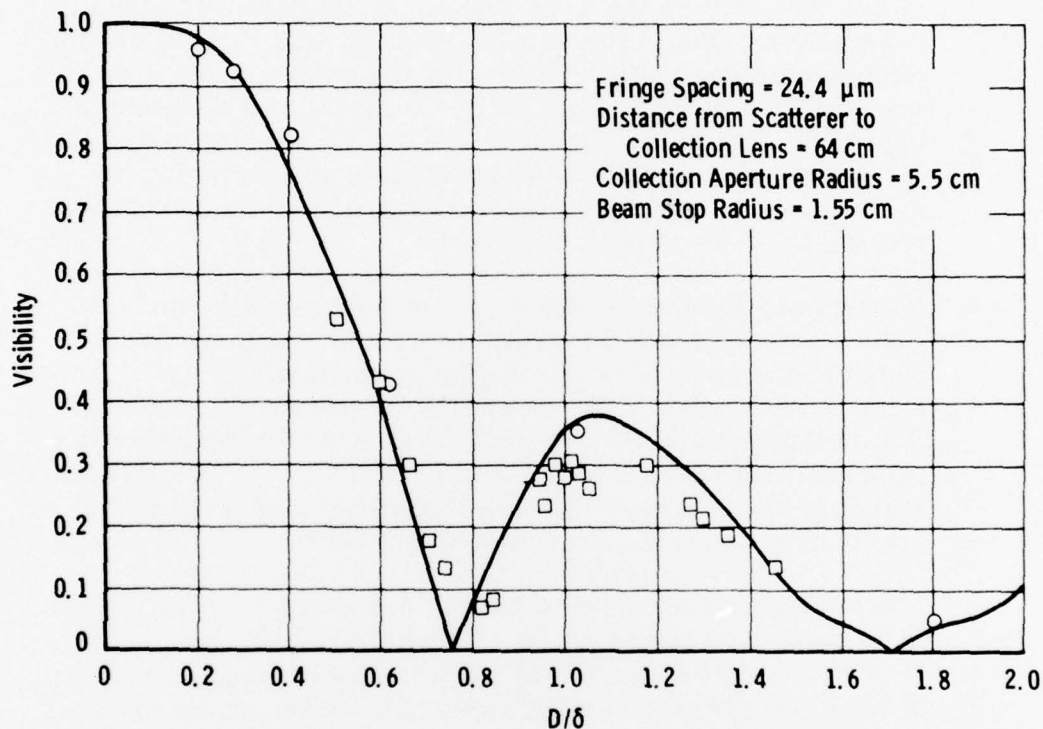


Figure 26. Theoretical and experimental comparison of visibility versus ratio of particle diameter to fringe spacing for a single circular beam stop.

2. The minimum size which may be measured with this technique has yet to be determined. One limitation is set by the slope of the curve relating to visibility and the ratio of particle size to fringe spacing. For particle diameters smaller than approximately $2/10$ of the fringe spacing, the slope of the visibility curve is not sufficiently great to accurately relate the visibility to the particle size (see Fig. 25). In addition, the minimum obtainable fringe spacing is limited by the maximum beam separation angle which can be obtained in a practical measuring

situation. It is believed that the maximum angle is approximately 12 deg, giving a fringe spacing of approximately five times the optical wavelength being used for the measurement. This limiting condition fixes the minimum measurable particle diameter at approximately one wavelength of the illuminating radiation.

3. Currently the visibility is measured when the particle is in either the $y = 0$ or the $z = 0$ plane. If the particles are all generally moving in the same direction, this may be accomplished electronically by orienting the optical system so that the particles pass through the $y = 0$ plane. An alternative approach, where the particles are not all moving in the same direction, is to consider the possibility of aperturing the system so that measurements are made only for particles moving in or near the $z = 0$ plane.
4. Background light collected by the optical system, including light scattered from the probe volume by small aerosols, which are always present, should be minimal (to avoid generation of shot noise in the detector) and relatively constant. Determining visibility requires measuring the height of the pedestal with respect to the background light. The present signal processor requires that the background be constant so that it may be measured and subtracted out.
5. The method assumes there is only one particle large enough to be measured in the probe volume at a time. If the density of particles in the system is high, creating a high probability of the occurrence of multiple particles in the probe volume, then some method must be used either to reject those waveforms caused by multiple particles or to investigate means for considering their influence on variations in the visibility from a single particle visibility function.
6. The EPA flame analyzer was designed to be interfaced with a four digit, particle size visibility processor. The data multiplexer can be programmed for simultaneous particle size and velocity measurements if desired.

5.0 THIRD COMPONENT OF VELOCITY

The purpose of this section is to outline conceptually the design criteria and systems considerations required for the inclusion of a third component velocity measurement. Several possible methods can be used to make this third component measurement. The various alternatives can take advantage of color separation, frequency separation, and off-axis or backscatter systems. Furthermore, either reference beam or dual-scatter techniques can be employed (Ref. 21). The argon-ion laser supplied with the EPA flame analyzer is capable of multiwavelength operation. In addition, an intra-cavity etalon has been supplied with the laser system. The purpose of this etalon is to increase the temporal coherence of the laser to allow for large mismatches in optical path. This is of particular importance with the reference beam systems. The principal argon laser wavelengths are 0.4880 and 0.5145 μm .

The choice of a measurement system for the third component for use in the rainbow furnace or similar environments is best filled by means of a backscatter reference beam system. Under more suitable viewing conditions, for example, when a large viewing port is available, an off-axis, dual-scatter system could be used. With the latter technique, distortions and tracking are primary considerations in their design. Figure 27 shows a single-beam system operating in the backscatter mode. If directionality were required, the Bragg cell would necessarily be employed. The argon laser is assumed to be running at the 0.4880- and 0.5145- μm wavelengths. Two sets of beams will therefore be generated and frequency shifted as previously described. Color separation techniques utilizing dielectric interference beam-splitters or careful positioning of a partially silvered mirror are used to remove the reference beam for the 0.4880- μm wavelength. A frequency-shifted beam with respect to the reference beam is allowed to pass out through the optical system and to be imaged in the probe volume by means of the output lens. Light is scattered from the particles within the probe volume, as before. The backscatter radiation is related to the velocity vector and the propagation vectors by the following equation:

$$f = f_0 + 1/2\pi (\vec{K}_s - \vec{K}_0) \cdot \vec{V} \quad (11)$$

where f_0 is the fundamental optical frequency, \vec{K}_s and \vec{K}_0 are the wave vectors of the scattered and incident beams, respectively, and \vec{V} is the

particle velocity vector. For operation in the backscatter mode, the Doppler shift becomes

$$f_d = K \cdot V_z \quad (12)$$

where V_z is the component of velocity in μsec along the optical axis and $K = 4 \text{ MHz/m/sec}$. This backscatter radiation is mixed with the reference beam to produce, in a square-law detector, the sum and difference frequencies. The measured current in the photodetector becomes

$$i = a [1/2 E_{10}^2 + E_{10} E_s \cos(\omega_{10} - \omega_s)t + 1/2 E_s^2] \quad (13)$$

where $\omega_{10}/2\pi$ and $\omega_s/2\pi$ are reference and signal beam frequencies, respectively, a is the proportionality constant, and E_{10} and E_s are the corresponding electric field strengths. Since frequency separation techniques are being used, the local oscillator frequency differs from the signal frequency under zero velocity conditions by an amount equal to the Bragg cell frequency. Furthermore, the difference in the color allows the frequency separation techniques to be applied independently of the two-component, dual-scatter signals using $0.5145\text{-}\mu\text{m}$ radiation.

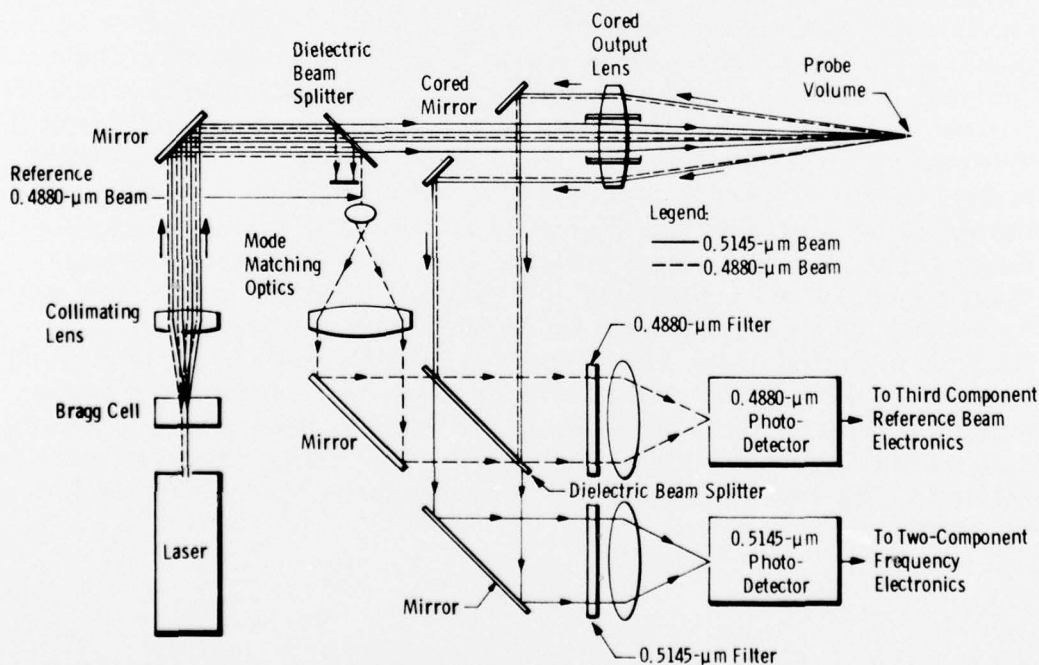


Figure 27. Proposed three-component velocimeter schematic.

A detailed analysis of system parameters such as spot size, system accuracy, bandwidth considerations due to the finite laser spot size and to the finite collection angle, and the effects of signal strength and signal-to-noise ratios has been reported (Ref. 20). One can generally conclude that the system accuracy is reduced with smaller spot sizes and larger receiver apertures because of the frequency spreading of the signal and the inability to accurately determine the line center. Also, a reduction in coherency between signal and the local oscillator beams can result in a requirement for larger reference or local oscillator beams to give the same signal-to-noise ratio. The minimum conversion gain permitted is limited by the allowable continuous wave (CW) or pulse current at the anode of the photomultiplier tube. Finally, the scattered particle density required for a given signal power varies inversely with the incident beam power density and the probe volume. A typical minimum particle density of 10^3 particles/cc is calculated for continuous signals, which are required for most reference beam processors. However, through the use of a burst-type counter this requirement can be reduced to measuring single-particle events, making the third-component particle density requirements consistent with the other velocity component counters and the particle-sizing electronics.

6.0 SUMMARY AND CONCLUSIONS

Theoretical analysis and confirming experimental data at the EPA "rainbow" furnace verify that the EPA flame analyzer velocimeter design under consideration was efficient for the application intended. Additional effort is required to include a third component so that three-dimensional turbulent flow characteristics may be measured. The viewport space limitations prevent the application of the off-axis, dual-beam concept. This essentially restricts the technique to the development of a reference beam, two-color system. Preliminary laboratory experiments have shown feasibility, and no major development difficulties are foreseen.

A prototype particle size/visibility processor has been developed and is currently being evaluated and calibrated in the laboratory. Preliminary results verify the application of the technique. Additional experiments are being planned in an operational wind tunnel to acquire the field experience necessary for the development of a second-generation system. A two-component visibility processor will result in further definition of the shapes of the particles being measured.

REFERENCES

1. Lennert, A. E., Brayton, D. B., Crosswy, F. L., et al.
"Summary Report of the Development of a Laser Velocimeter to be Used in AEDC Wind Tunnels." AEDC TR-70-101 (AD871321), July 1970.
2. Brayton, D. B. and Goethert, W. H. "A New Dual-Scatter Doppler-Shift Velocity Measuring Technique." ISA Transactions, Volume 10, No. 1, 1971, pp. 40-50.
3. Rudd, M. J. "A New Theoretical Model for the Laser Dopplermeter." Journal of Scientific Instruments (Journal of Physics E), Series 2, Vol. 2, 1969, pp. 55-58.
4. Penney, C. M. "Differential Doppler Velocity Measurements." IEEE Journal of Quantum Electronics, Vol. QE5, No. 6, pp. 318-319.
5. Durst, F. and Whitelaw, J. H. "Optimization of Optical Anemometers." Proceedings of the Royal Society of London, Series A, Vol. 324, 1971, pp. 157-181.
6. Mayo, W. T., Jr. "Simplified Laser Doppler Velocimeter Optics." Journal of Physics E: Scientific Instruments, Vol. 3, March 1970, pp. 235-237.
7. Durst, F. "Scattering Phenomena and Their Application in Optical Anemometry." Journal of Applied Mathematics and Physics (ZAMP), Vol. 24, 1973, pp. 619-643.
8. Farmer, W. M. "The Interferometric Observation of Dynamic Particle Size, Velocity and Number Density." PhD Dissertation, University of Tennessee, Knoxville, 1973.
9. Farmer, W. M. "Measurement of Particle Size, Number Density, and Velocity Using a Laser Interferometer." Applied Optics, Vol. 11, November 1972, pp. 2603-2612.
10. Roberds, D. W. "Electronic Instrumentation for Interferometric Particle Sizing." PhD Dissertation, University of Tennessee, Knoxville, 1975.

11. Fried, D. L. "Optical Heterodyne Detection of an Atmospherically Distorted Signal Wave Front." Proceedings of the IEEE, Vol. 55, No. 1, January 1967, pp. 57-67.
12. Hodara, H. "Laser Wave Propagation Through the Atmosphere." Proceedings of the IEEE, Vol. 54, No. 3, March 1966, pp. 368-375.
13. Treacy, E. B. "An Analysis of Some Factors Affecting the Accuracy of Laser Doppler Velocimetry." Instrumentation in the Aerospace Industry, Vol. 17, 1971, pp. 165-173.
14. Goethert, W. H. "Laser Doppler Velocimeter Dual-Scatter Probe Volume." AEDC-TR-71-85 (AD727005), July 1971.
15. Kogelnik, H. "Imaging of Optical Modes - Resonators with Internal Lenses." Bell System Technical Journal, Vol. 44, March 1965, pp. 455-494.
16. Durst, F. and Stevenson, W. H. "The Influence of Gaussian Beam Effects on the Spectral Nature of Laser Doppler Signals." Proceedings of the Minnesota Symposium on Laser Anemometry, October 22-24, 1975.
17. Lennert, A. E., Crosswy, F. L., and Kalb, H. T. "Application of the Laser Velocimeter for Trailing Vortex Measurements." AEDC-TR-74-26 (ADA002151), December 1974.
18. Farmer, W. M. and Hornkohl, J. O. "Two-Component, Self Aligning Laser Vector Velocimeter." Applied Optics, Vol. 12, No. 11, November 1973, pp. 2636-2640.
19. Chu, W. P. and Mauldin, L. E. "Bragg Diffraction of Light by Two Orthogonal Ultrasonic Waves in Water." Applied Physics Letters, Vol. 22, No. 11, June 1973, pp. 557-559.
20. Roberds, D. W., Farmer, W. M., and Lennert, A. E. "Interferometric Instrumentation for Particle Size Analysis." AEDC-TR-74-82 (ADA006136), February 1975.
21. Davis, Donald T. "Analysis of a Laser Doppler Velocimeter." ISA Transactions, Vol. 7, No. 1, 1968, pp. 43-51.

NOMENCLATURE

$2b$	Input beam diameter, Fig. 3
$2b_o$	Characteristic dimension of probe volume
C	Speed of sound in diffracting medium
D	Beam separation at output lens
d_i, d_o	Input and output beam diameters, respectively, Eq. (10)
F_P, F_C	Primary and collimator focal lengths, respectively
F_i, F_o	Input and output focal lengths, respectively, Eq. (10)
F_L	Focal length of lens, Eq. (4)
f_b	Driver frequency
f_m	Modulation frequency of ultrasonic wave
f_o	Fundamental optical frequency
\vec{K}_s, \vec{K}_o	Wave vectors of scattered and incident beams, respectively
LED	Light-emitting diode
M	Magnification
N	Order of diffraction
\vec{V}	Velocity of sound in water
V_z	Component of velocity along optical axis, μsec
α	Angle between two crossed Gaussian beams
β	Angle between crossed beams in Gaussian mode
δ	Fringe spacing in probe volume

Λ	Wavelength of sound in diffracting medium
λ	Wavelength of light
ϕ	Angle from optical axis of first diffraction minimum, Eq. (6)
$\omega_{10}/2\pi$	Reference beam frequency
$\omega_s/2\pi$	Reference signal frequency